Lappeenranta University of Technology
Department of Mechanical Engineering

The Dynamic Analysis of a Human Skeleton Using the Flexible Multibody Simulation Approach

The topic of the Thesis has been confirmed by the Department Council of the Department of Mechanical Engineering on 1st November, 2006.

Supervisors: Dr.Tech.,Professor Aki Mikkola
Dr.Tech.,Docent Asko Rouvinen

Lappeenranta, 9th November, 2006

Rami Abdullah Mohammad Al Nazer
Väinölänkatu 27 B 14
Lappeenranta 5310
Finland
Tel: +358-50-9253226
rami.al.nazer@lut.fi

ABSTRACT

Author:	Rami Al Nazer
Title:	**The Dynamic Analysis of a Human Skeleton Using the Flexible Multibody Simulation Approach**
Department:	Mechanical Engineering
Place:	Lappeenranta
Year:	2006

Master's thesis. Lappeenranta University of Technology

58 pages, 33 figures and 6 tables

Supervisors:	Dr.Tech.,Professor Aki Mikkola and Dr.Tech.,Docent Asko Rouvinen
Keywords:	Flexible multibody dynamic, human lower limb model, bone strength

The human motion study, which relies on mathematical and computational models in general, and multibody dynamic biomechanical models in particular, has become a subject of many recent researches. The human body model can be applied to different physical exercises and many important results such as muscle forces, which are difficult to be measured through practical experiments, can be obtained easily. In this work, a human skeletal lower limb model consisting of three bodies is built using the flexible multibody dynamic simulation approach. The floating frame of reference formulation is used to account for the flexibility in the bones of the human lower limb model. The main reason of considering the flexibility in the human bones is to measure the strains in the bone result from different physical exercises. It has been perceived that the bone under strain will become stronger in order to cope with the exercise. On the other hand, the bone strength is considered an important factor in reducing the bone fractures.

The simulation approach and model developed in this work are used to measure the bone strain results from applying raising the sole of the foot exercise. The simulation results are compared to the results available in literature. The

comparison shows good agreement. This study sheds the light on the importance of using the flexible multibody dynamic simulation approach to build human biomechanical models, which can be used in developing some exercises to achieve the optimal bone strength.

ACKNOWLEDGEMENTS

This research was carried out in the Department of Mechanical Engineering, Lappeenranta University of Technology, between May 2006 and November 2006.

This thesis would not have been completed without the support of my great supervisor, Aki Mikkola, a Professor in the Mechatronics and Virtual Engineering Laboratory. Although I have worked hard to complete this thesis, the final product came about as a result of his enthusiastic overtures. With him I had many wonderful and persuasive discussions. To him I owe more than words can describe.

I am also grateful to the second supervisor of this thesis Dr. Asko Rouvinen for his valuable comments and advice.

I am especially thankful to my friend Mr. Timo Rantalainen, a researcher in the department of biology of physical activity in University of Jyvaskyla, for his valuable comments and advice as well as enthusiastic support at all stages of the work.

I would like also to thank my colleague at the Department of Mechanical Engineering Mr. Tuomas Rantalainen for his assistance and help.

Last but no least, my family has been always the source of love and support in my life. My father Abdullah, is always the source of wisdom in my life. My mother Tagreed, forever I am grateful. My brothers Romel, Ramez and Mohammed and my sister Raya, with your care and love you make the hard easy infront of me.

NOMENCLATURE

Abbreviations

ADAMS	Automatic Dynamic Analysis of Mechanical Systems
CMS	Component Mode Synthesis
CT	Computerized Tomography
DAE	Differential Algebraic Equations
DOF	Degree of Freedom
MRI	Magnetic Resonance Imaging
VIVO	Latin expression refers to experimentation done on a living body

Symbols

$\mathbf{A}^i$	Transformation matrix of the flexible body *i* coordinate system
$\mathbf{A}^i_\theta$	Matrix results from taking the derivative of the transformation matrix of the flexible body *i* coordinate system with respect to the rotation angle
$\mathbf{a}^i_k$	Eigenvectors correspond to the eigenvalues of the flexible body *i*
$\mathbf{B}^{ij}$	Boolean transformation matrix defines the vector of element *ij* nodal coordinates in terms of the total vector of elastic nodal coordinates of the flexible body *i*
$\mathbf{B}^i_r$	Boolean reference transformation matrix defines the reference conditions applied to the flexible body *i*
$\mathbf{C}$	Vector of linearly independent constraint equations of the multibody system
$\mathbf{C}^{ij}$	2 x 2 transformation matrix defines the orientation of the element *j* coordinate system with respect to the flexible body *i* coordinate system
$\mathbf{C}_\mathbf{q}$	Jacobian matrix
$\mathbf{D}^i$	Strain-displacement matrix of the flexible body *i*
$\mathbf{E}^i$	Symmetric matrix of the elastic coefficients of the flexible body *i*
$\mathbf{e}^{ij}$	Vector of the element *ij* nodal coordinates

$\mathbf{e}^i$	Vector of the elastic nodal coordinates of the flexible body *i*
$\mathbf{e}_o^{ij}$	Vector of the nodal coordinates of the element *ij* in the undeformed state
$\mathbf{e}_f^{ij}$	Vector of the nodal coordinates of the element *ij* in the deformed state
$\ddot{\mathbf{e}}^i$	Acceleration vector of the elastic nodal coordinates of the flexible body *i*
$\mathbf{F}^i$	External force acting on a flexible body *i*
$\mathbf{I}$	2 x 2 identity matrix
$\mathbf{I}_1^i$	Vector defines the moment of the body mass about the axes of the flexible body *i* coordinate in the undeformed state
$\tilde{\mathbf{I}}$	Skew symmetric matrix
$\mathbf{K}^i$	Generalized stiffness matrix associated with the generalized coordinates of the flexible body *i*
$\mathbf{K}_{ff}^i$	Symmetric positive definite stiffness matrix associated with the generalized elastic coordinates of the flexible body *i*
$\mathbf{K}_p^i$	Modal stiffness matrix of the flexible body *i*
$\hat{\mathbf{K}}^i$	Craig-Bampton stiffness transformation matrix of the flexible body *i*
k^i	Modal stiffness coefficients of the flexible body *i*
$\mathbf{M}^i$	Mass matrix of the flexible body *i*
$\mathbf{M}_p^i$	Modal mass matrix of the flexible body *i*
$\hat{\mathbf{M}}^i$	Craig-Bampton mass transformation matrix of the flexible body *i*
m	Number of low frequency mode shapes
m^i	Mass of the flexible body *i*
m_d	Number of uncoupled differential equations
$\hat{m}^i$	Modal mass coefficients of the flexible body *i*
$\mathbf{m}_{ff}^i$	Constant submatrix of the mass matrix associated with the elastic flexible body *i* coordinates

$\mathbf{m}_{RR}^{i}$	Submatrix of the mass matrix associated with the translational coordinates of the flexible body *i* coordinate system
$\mathbf{m}_{Rf}^{i}$	Submatrix of the mass matrix represents the coupling between the flexible body *i* translational reference motion and the elastic deformation
$\mathbf{m}_{R\theta}^{i}$	Submatrix of the mass matrix represents the coupling between the flexible body *i* reference translational and rotational coordinates
$\mathbf{m}_{\theta f}^{i}$	Submatrix of the mass matrix represents the coupling between the flexible body *i* rotational reference motion and the elastic deformation
$\mathbf{m}_{\theta\theta}^{i}$	Constant submatrix of the mass matrix associated with the flexible body *i* rotational reference coordinates
$(m_{\theta\theta}^{i})_{ff}$	Scalar represents the change in the mass moment of inertia of the flexible body *i* due to deformation
$(m_{\theta\theta}^{i})_{rf}$	Scalar represents the change in the mass moment of inertia of the flexible body *i* due to deformation
$(m_{\theta\theta}^{i})_{rr}$	Scalar represents the mass moment of inertia of the flexible body *i* in the undeformed state about perpendicular axis to the plane
$\hat{\mathbf{N}}^{i}$	Transformation matrix transforms the modal coordinates of the Craig-Bampton modes of the flexible body *i* to an equivalent orthogonal modal coordinates
n	Number of generalized coordinates of the multibody system
n_b	Total number of the bodies in the planar multibody dynamic system
n_c	Number of the constraint equations of the multibody system
n_f	Number of the elastic coordinates of the flexible body *i*
n_n	Number of the elastic nodal coordinates of the flexible body *i*
O^{i}	Origin of the flexible body *i* coordinate system
O^{ij}	Origin of the element *j* coordinate system
P^{i}	Arbitrary point on the flexible body *i*

P^{ij}	Arbitrary point on element *ij*
$\mathbf{p}^i$	Vector of the modal coordinates of the flexible body *i*
$\mathbf{p}_f^i$	Vector of the modal elastic nodal coordinates of the flexible body *i*
$\mathbf{p}_r^i$	Vector of the modal reference coordinates of the flexible body *i*
$\hat{\mathbf{p}}^i$	Vector of the modal coordinates of the Craig-Bampton modes of the flexible body *i*
$\hat{\mathbf{p}}_C^i$	Vector of modal coordinates of the Craig-Bampton constraint modes of the flexible body *i*
$\hat{\mathbf{p}}_N^i$	Vector of modal coordinates of the Craig-Bampton fixed boundary normal modes of the flexible body *i*
$\mathbf{Q}^i$	Vector of the generalized elastic and external forces of the flexible body *i*
$\mathbf{Q}_e^i$	Vector of generalized external forces associated with the generalized coordinates of the flexible body *i*
$\mathbf{Q}_f^i$	Vector of generalized external forces associated with elastic coordinates of the flexible body *i*
$\mathbf{Q}_R^i$	Vector of generalized external forces associated with the translational reference coordinates of the flexible body *i*
$\mathbf{Q}_v^i$	Quadratic velocity vector of the flexible body *i*
$\mathbf{Q}_\theta^i$	Vector of generalized external forces associated with the rotational reference coordinates of the flexible body *i*
$(\mathbf{Q}_v^i)_f$	Quadratic velocity vector associated with the elastic coordinates of the flexible body *i*
$(\mathbf{Q}_v^i)_R$	Quadratic velocity vector associated with the translational reference coordinates of the flexible body *i*
$(\mathbf{Q}_v^i)_\theta$	Quadratic velocity vector associated with the rotational reference coordinates of the flexible body *i*
$\mathbf{q}$	Vector of the total multibody system generalized coordinates

$\mathbf{q}^i$	Generalized coordinates system of the flexible body *i*
$\mathbf{q}_f^i$	Vector of elastic coordinates of the flexible body *i*
$\mathbf{q}_r^i$	Vector of reference coordinates of the flexible body *i*
$\dot{\mathbf{q}}^i$	Velocity of the generalized coordinates system of the flexible body *i*
$\dot{\mathbf{q}}_f^i$	Velocity of the generalized elastic coordinates of the flexible body *i*
$\ddot{\mathbf{q}}^i$	Acceleration of the generalized elastic coordinates of the flexible body *i*
$\mathbf{R}^i$	Vector of the translation of the origin of the flexible body *i* coordinate system with respect to the global coordinate
$\dot{\mathbf{R}}^i$	Vector of the translational velocities of the origin of the flexible body *i* with respect to the global coordinate system
$\mathbf{r}_P^i$	Position vector of any arbitrary point on the flexible body *i* with respect to the global coordinate system
$\mathbf{r}_P^{ij}$	Position vector for any arbitrary point on the element *ij* with respect to the global coordinate system
$\dot{\mathbf{r}}_P^i$	Velocity vector of any arbitrary point on the flexible body *i* with respect to the global coordinate system
$\ddot{\mathbf{r}}_P^i$	Acceleration vector of any arbitrary point on the flexible body *i* with respect to the global coordinate system
$\mathbf{S}^i$	Space dependent shape matrix of the flexible body *i*
$\mathbf{S}^{ij}$	Space dependant shape matrix of the element *ij*
$\tilde{\mathbf{S}}^i$	Constant skew symmetric matrix of the flexible body *i*
T^i	Kinetic energy of the flexible body *i*
t	time
$\bar{\mathbf{u}}^i$	Position vector of any arbitrary point on the flexible body *i* with respect to the body coordinate system
$\bar{\mathbf{u}}_f^i$	Deformed position vector of any arbitrary point on the flexible body *i* with respect to the body coordinate system

$\bar{\mathbf{u}}_o^i$ Undeformed position vector of any arbitrary point on the flexible body *i* with respect to the body coordinate system

$\bar{\mathbf{u}}^{ij}$ Vector of the assumed displacement field of the nodal coordinates of the element *ij* with respect to the flexible body *i* coordinate system

V^i Volume of the flexible body *i*

$\delta \mathbf{W}_e^i$ Virtual work of external forces acting on a flexible body *i*

$\delta \mathbf{W}_s^i$ Virtual work done by the elastic forces acting on a flexible body *i*

$\mathbf{w}^{ij}$ Vector of the assumed displacement field of the nodal coordinates of the element *ij* with respect to the element *ij* coordinate system

$\mathbf{X}_1\mathbf{X}_2$ Global coordinate system

$\mathbf{X}_1^i\mathbf{X}_2^i$ Flexible body *i* coordinate system

$\mathbf{X}_1^{ij}\mathbf{X}_2^{ij}$ Element *j* coordinate system

Greek Letters

θ^i Orientation angle of the flexible body *i* coordinate system with respect to the global coordinate system

$\dot{\theta}^i$ Angular velocity of the flexible body *i* coordinate system with respect to the global coordinate system

ρ^i Density of the flexible body *i*

$\boldsymbol{\sigma}^i$ Stress vector of the flexible body *i*

$\boldsymbol{\varepsilon}^i$ Strain vector of the flexible body *i*

$\boldsymbol{\lambda}$ Vector of Lagrange multipliers

ω_k^i Eigenvalues or natural frequencies associated with each nodal coordinate of the flexible body *i*

$\overline{\boldsymbol{\Phi}}^i$ Modal transformation matrix

$\boldsymbol{\Phi}^i$ Modal transformation matrix for the total vector of the generalized coordinates system of the flexible body *i*

$\boldsymbol{\Psi}^i$ Craig-Bampton transformation matrix of the vector of generalized coordinates system of the flexible body *i*

$\boldsymbol{\Psi}^i_{IC}$	Craig-Bampton transformation matrix of the vector of elastic nodal coordinates of the flexible body *i* or the ineterior DOF in the constraint modes
$\boldsymbol{\Psi}^i_{IN}$	Craig-Bampton transformation matrix of the vector of elastic nodal coordinates of the flexible body *i* or the ineterior DOF in the normal modes
λ^i	Eigenvalues or natural frequencies associated with each modal coordinate of the Craig-Bampton modes of the flexible body *i*
$\boldsymbol{\Omega}^i$	Orthogonal eigenvectors correspond to the eigenvalues associated with each modal coordinate of the Craig-Bampton modes of the flexible body *i*

Contents

1. INTRODUCTION

Multibody dynamic approach is a mathematical tool that can be used to model different mechanical and structural systems. For instance, such systems included under the definition of multibody systems comprise robots, manipulators, vehicles and human skeleton. **Figure 1.1** illustrates a general multibody system shown in abstract form.

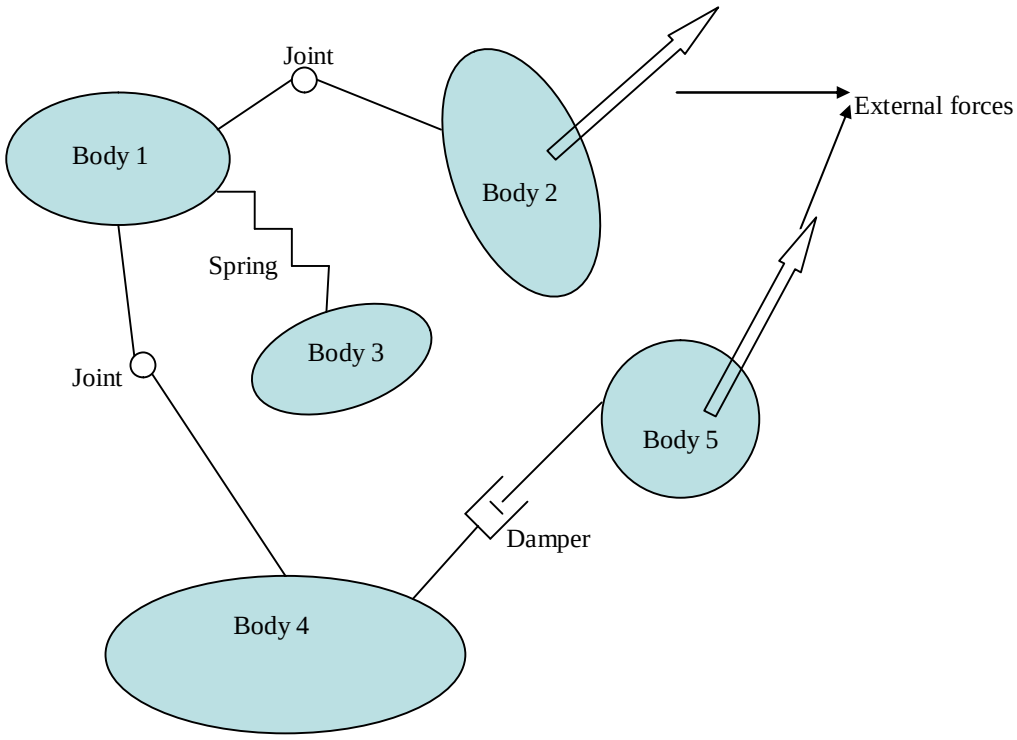

Figure 1.1. General multibody system.

As depicted from **Figure 1.1**, a multibody system consists of several bodies, which can be rigid, flexible or combination of them. Those bodies are connected together by means of kinematic joints described by constraint equations. The forces applied over the multibody system bodies may be a result of springs, dampers, actuators or any external applied forces such as gravitational forces. The biomechanical human models are typically more complicated than technical multibody systems, as they involve a larger variety of joint types and body forms, complex actuators in the form of muscles, connected groups of bones and

neighbouring soft tissue [1]. Recently, multibody dynamic approach has been used extensively in modelling human skeleton. Several important results can be depicted from the human skeleton model. For instance, the internal forces in the skeleton and muscular reactions. The key issue from using multibody dynamic in human skeleton modelling is that there are no experimental methodologies capable of measuring these depicted parameters [2]. In other words, using the multibody dynamic model of the human skeleton, several important parameters can be measured, which are of a major importance in many scientific fields such as, medicine, sports and biomechanical engineering. In this particular study, a part from human skeleton which is the lower limb shown in **Figure 1.2**, is modelled using multibody dynamic approach.

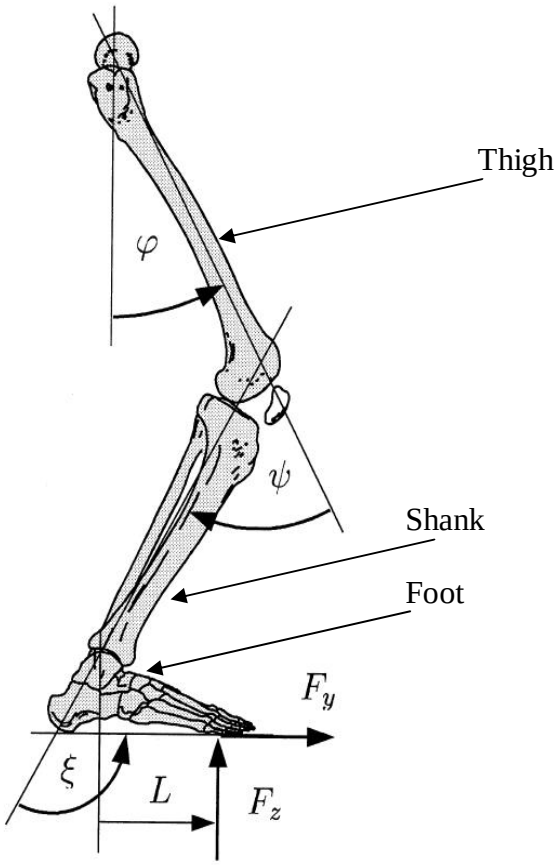

Figure 1.2. Lower limb [3].

It can be noticed from **Figure 1.2** that the lower limb consists of several bodies connected to each other by means of joints, with external forces applied on these

bodies. Therefore by comparing the lower limb shown in **Figure 1.2** with the general multibody system shown in **Figure 1.1**, one may notice that the multibody dynamic approach can be applied to model the lower limb. For simplicity, the lower limb model will be consisting of three bodies; the thigh, the shank and the foot. The motivation of this study is to calculate the strains in the lower limb bones. It has been perceived that the bone under strain will become stronger in order to cope with the exercises induced loading. The strength of the bone is considered an important factor in reducing the risk of bone osteoporotic fracture, which is mainly, affecting the aged people. Therefore, many sport exercises can be developed, in order to maintain or increase the bone strength [4]. In order to calculate the strains in the lower limb bone, the bone has to be modelled as a flexible body. Many previous studies have been conducted in human skeleton modelling. In the work of Bei and Fregly (2004) a detailed musculoskeletal multibody model is created in order to predict muscle forces and contact pressures simultaneously in a knee joint [5]. In this model, the flexible contact of the joint is combined with the rigid body dynamics of two bones. Silva *et al*. [6] have included the natural boundary conditions for joints in a multibody model in order to prevent physically unnatural positions of limbs when modelling human kinematics. Another specified model of a particular area of interest is found in Reference [7] where muscles are studied. A combined biomechanical model including three rigid bones and active muscles to simulate real human movements in a vertical jump is studied in Reference [3]. In order to verify and perform an inverse dynamical problem, the motion of a limb is captured using cameras [8]. A number of articles have been published on the analysis of the kinematics and motion of the entire human body, e.g. [9-11]. The natural coordinates approach has been applied in many cases when whole human body models are studied. Kraus *et al*. [1] have built a human model including over 100 degrees of freedom. In a model of this size, the number of parameters is high and they need to be systematically determined. In reference [12], the parameters area studied for the model applied in a vehicle crash simulation. Crash test models have been under intensive research and many studies are related to this field. In multibody application topics related to the computational techniques are often important and interesting. In Reference [13], the authors study the problem related to the

solution of differential-algebraic equations (**DAE**) in a multibody model defining an android in a crash test. In all of the previous studies, the bones were modelled as rigid bodies. Therefore, these models can not be used to calculate the bone strains. In this study, the lower limb bones are modelled as flexible bodies. Flexibility in multibody dynamic models can be taken into account through several ways. In this study, floating frame of reference [14-16] is used to account for the flexibility in the lower limb model.

1.1 Scope of the Work

Many parameters in the human body such as muscle forces and their net moments force about the anatomical joints are difficult to be measured through real experiments. Thus, using computer tools to model the human body becomes an important issue. In this work, a skeletal lower limb is modelled using the flexible multibody dynamic approach. The flexibility has been taken into account in order to measure the strains in the bone, which play a major role in strengthening the bones. The strength of the bone is considered an important resistant factor against the metabolic bone diseases. The main purpose of this work is to show the capability of the flexible multibody dynamic approach in modelling the human skeletal through measuring the strains in the bone. Not all the important issues in human skeletal modelling are covered in this work. Aspects, such as neural control system or muscle tendons modelling are not addressed here, as they have negligible effects on the main purpose of this work.

2. FLOATING FRAME OF REFERENCE FORMULATION

In theory all the bodies are flexible and have infinite number of degree of freedom. However in practice there are number of ways to account for flexibility. In this chapter, a method to take into account the flexibility of the bodies in multibody dynamic system is explained in details. This method is called the floating frame of reference.

In the following sections of this chapter a detailed formulation of the equations of motion based on the floating frame of reference for a planar flexible body is presented. For a better accuracy in modelling the elastic deformation in the flexible body, the finite element method is used in the floating frame of reference formulation. This method that implies discretization the flexible body into elements and each element consists of number of nodes is explained in later sections in this chapter. Due to the high number of elastic coordinates resulted from discretization of the flexible body into finite number of elements, modal reduction method is presented at the end of this chapter to reduce the number of the elastic coordinates.

2.1 Description of Kinematics

The floating frame of reference formulation is based on the use of two coordinate systems; reference and elastic coordinate systems. **Figure 2.1** shows the floating frame of reference coordinate systems, for a planar flexible body *i*.

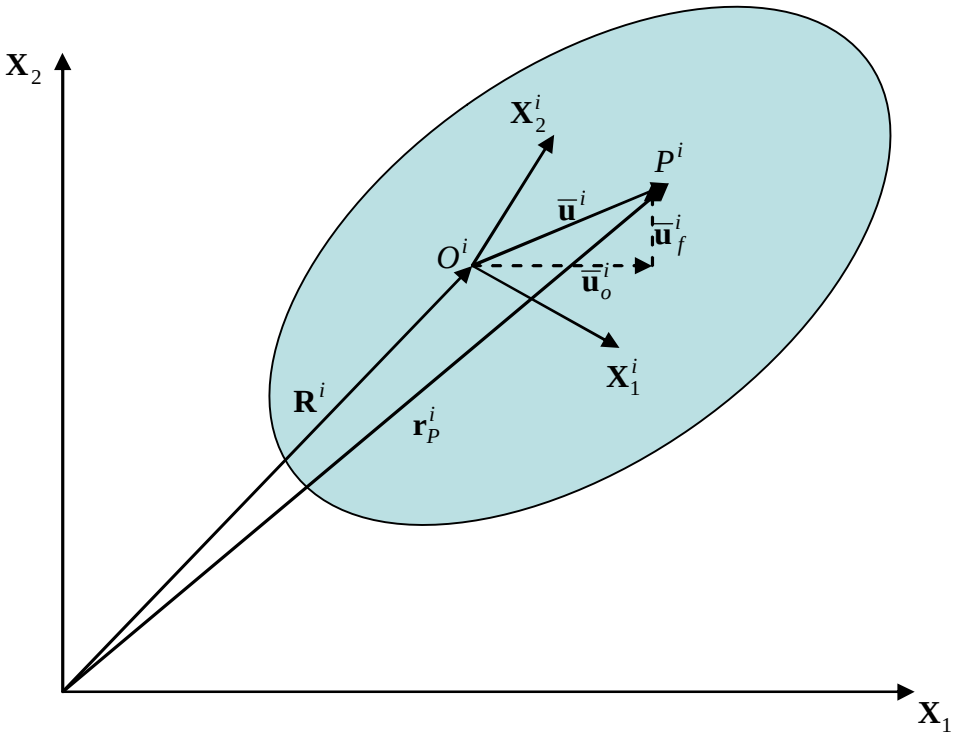

Figure 2.1. Coordinates for a planar flexible body *i* in the floating frame of reference formulation.

The generalized coordinates system of the flexible body *i* shown in the previous figure can be expressed as follows:

$$\mathbf{q}^i = \begin{bmatrix} \mathbf{q}_r^i & \mathbf{q}_f^i \end{bmatrix} \tag{2.1}$$

where $\mathbf{q}_r^i$ is the vector of reference coordinates, which describes the translation and rotation of the flexible body *i* coordinate system $\mathbf{X}_1^i\mathbf{X}_2^i$ with respect to the global coordinate system $\mathbf{X}_1\mathbf{X}_2$ and $\mathbf{q}_f^i$ is the vector of elastic coordinates, which describes the elastic deformation of the flexible body *i* with respect to the body coordinate system. The vector $\mathbf{q}_r^i$ can be expressed as follows:

$$\mathbf{q}_r^i = \begin{bmatrix} \mathbf{R}^i & \theta^i \end{bmatrix}^T \tag{2.2}$$

where $\mathbf{R}^i$ is the vector that describes the translation of the origin O^i of the flexible body *i* coordinate system with respect to the global coordinate system and θ^i is the

orientation angle of the flexible body *i* coordinate system with respect to the global coordinate system. The vector $\mathbf{q}_f^i$ in **Eq 2.1** can be expressed as follows:

$$\mathbf{q}_f^i = \begin{bmatrix} \mathbf{q}_{f1}^i & \mathbf{q}_{f2}^i & \cdots & \mathbf{q}_{fn_f}^i \end{bmatrix}^T \tag{2.3}$$

where n_f is the number of the elastic coordinates. The vector $\bar{\mathbf{u}}^i$ shown in the previous figure, describes the position of any arbitrary point P^i on the flexible body *i* with respect to the body coordinate system. The vector can be expressed as follows:

$$\bar{\mathbf{u}}^i = \bar{\mathbf{u}}_o^i + \bar{\mathbf{u}}_f^i \tag{2.4}$$

where $\bar{\mathbf{u}}_o^i$ is the vector describes the undeformed position of point P^i with respect to the body coordinate system and $\bar{\mathbf{u}}_f^i$ is the vector describes the deformed position of point P^i with respect to the body coordinate system. The vector $\bar{\mathbf{u}}_f^i$ can be expressed by means of shape function matrix and elastic coordinates as follows:

$$\bar{\mathbf{u}}_f = \mathbf{S}^i \mathbf{q}_f^i \tag{2.5}$$

where $\mathbf{S}^i$ is a space dependent shape matrix, which identify the shape of the deformation for each point in the flexible body *i*. Substituting **Eq 2.5** into **Eq 2.4** yields to the following equation:

$$\bar{\mathbf{u}}^i = \bar{\mathbf{u}}_o^i + \mathbf{S}^i \mathbf{q}_f^i \tag{2.6}$$

The vector $\mathbf{r}_P^i$ shown in the previous figure, describes the position of point P^i with respect to the global coordinate system. The vector can be expressed in the following equation:

$$\mathbf{r}_P^i = \mathbf{R}^i + \mathbf{A}^i \bar{\mathbf{u}}^i = \mathbf{R}^i + \mathbf{A}^i (\bar{\mathbf{u}}_o^i + \mathbf{S}^i \mathbf{q}_f^i) \tag{2.7}$$

where $\mathbf{A}^i$ is the transformation matrix, which describes the rotation of the flexible body *i* coordinate system with respect to the global coordinate system. It can be expressed as follows:

$$\mathbf{A}^i = \begin{bmatrix} \cos\theta^i & -\sin\theta^i \\ \sin\theta^i & \cos\theta^i \end{bmatrix} \tag{2.8}$$

Description of Velocity

In order to get the velocity equations, **Eq 2.7** has to be differentiated with respect to the time. This yields to the velocity vector of any arbitrary point on the flexible body *i* with respect to the global coordinate system, which can be expressed as follows:

$$\dot{\mathbf{r}}_P^i = \dot{\mathbf{R}}^i + \dot{\mathbf{A}}^i \bar{\mathbf{u}}^i + \mathbf{A}^i \dot{\bar{\mathbf{u}}}^i \tag{2.9}$$

where $\dot{\mathbf{R}}^i$ is the vector of translational velocities of the origin O^i of the flexible body *i* with respect to the global coordinate system and $\dot{\bar{\mathbf{u}}}^i$ can be obtained by differentiating **Eq 2.6** with respect to the time. This yields to the following equation:

$$\dot{\bar{\mathbf{u}}}^i = \mathbf{S}^i \dot{\mathbf{q}}_f^i \tag{2.10}$$

where $\dot{\mathbf{q}}_f^i$ is the velocity of the generalized elastic coordinates. One may notice here, that differentiating the vector $\bar{\mathbf{u}}_o^i$ with respect to the time, yields to zero as the vector is constant. The matrix $\dot{\mathbf{A}}^i$ in **Eq 2.9** can be expressed as follows:

$$\dot{\mathbf{A}}^i = \mathbf{A}_\theta^i \mathbf{S}^i \dot{\theta}^i \tag{2.11}$$

where $\dot{\theta}^i$ is the angular velocity of the flexible body *i* coordinate system with respect to the global coordinate system and $\mathbf{A}_\theta^i$ is the matrix results from taking the derivative of the transformation matrix described in **Eq 2.8** with respect to the rotation angle θ^i. The matrix can be expressed as follows:

$$\mathbf{A}_\theta^i = \begin{bmatrix} -\sin\theta^i & -\cos\theta^i \\ \cos\theta^i & -\sin\theta^i \end{bmatrix} \tag{2.12}$$

Subsisting **Eq 2.10** into **Eq 2.9** yields to the following equation:

$$\dot{\mathbf{r}}_P^i = \dot{\mathbf{R}}^i + \dot{\mathbf{A}}^i \bar{\mathbf{u}}^i + \mathbf{A}^i \mathbf{S}^i \dot{\mathbf{q}}_f^i \tag{2.13}$$

The preceding equation can be simplified for later derivation purpose, by rewriting the central term on the right hand side as follows:

$$\dot{\mathbf{A}}^i \bar{\mathbf{u}}^i = \mathbf{B}^i \dot{\theta}^i \tag{2.14}$$

where $\mathbf{B}^i$ can be expressed as follows:

$$\mathbf{B}^i = \mathbf{A}_\theta^i \bar{\mathbf{u}}^i \tag{2.15}$$

Substituting **Eq 2.14** into **Eq 2.13** yields to the following equation:

$$\dot{\mathbf{r}}_P^i = \dot{\mathbf{R}}^i + \mathbf{B}^i \dot{\theta}^i + \mathbf{A}^i \mathbf{S}^i \dot{\mathbf{q}}_f^i \tag{2.16}$$

The velocity vector defined in the preceding equation can be described in a partitioned form as follows:

$$\dot{\mathbf{r}}_P^i = \begin{bmatrix} \mathbf{I} & \mathbf{B}^i & \mathbf{A}^i \mathbf{S}^i \end{bmatrix} \begin{bmatrix} \dot{\mathbf{R}}^i \\ \dot{\theta}^i \\ \dot{\mathbf{q}}_f^i \end{bmatrix} \tag{2.17}$$

where $\mathbf{I}$ is the 2 x 2 identity matrix. **Equation 2.17** can be also expressed as follows:

$$\dot{\mathbf{r}}_P^i = \mathbf{L}^i \dot{\mathbf{q}}^i \tag{2.18}$$

where $\dot{\mathbf{q}}^i$ is the velocity of the generalized coordinates system of the flexible body i and $\mathbf{L}^i$ is a matrix which can be expressed as follows:

$$\mathbf{L}^i = \begin{bmatrix} \mathbf{I} & \mathbf{B}^i & \mathbf{A}^i \mathbf{S}^i \end{bmatrix} \tag{2.19}$$

Description of Acceleration

Recalling back **Eq 2.18**, and differentiating it with respect to time, the acceleration of point P^i with respect to the global coordinate system can be expressed as follows:

$$\ddot{\mathbf{r}}_P^i = \dot{\mathbf{L}}^i \dot{\mathbf{q}}^i + \mathbf{L}^i \ddot{\mathbf{q}}^i \tag{2.20}$$

where $\ddot{\mathbf{q}}^i$ is the acceleration of the generalized elastic coordinates and $\dot{\mathbf{L}}^i$ can be expressed as follows:

$$\dot{\mathbf{L}}^i = \begin{bmatrix} \mathbf{0} & \dot{\mathbf{B}}^i & \dot{\mathbf{A}}^i \mathbf{S}^i \end{bmatrix} \tag{2.21}$$

where $\mathbf{0}$ is a 2 x 2 zero matrix and $\dot{\mathbf{B}}^i$ can be obtained by differentiating **Eq 2.15** with respect to the time which yields to the following equation:

$$\dot{\mathbf{B}}^i = -\mathbf{A}^i \bar{\mathbf{u}}^i \dot{\theta}^i + \mathbf{A}_\theta^i \mathbf{S}^i \dot{\mathbf{q}}_f^i \tag{2.22}$$

2.2 Kinematic Constraints

Multibody dynamic system consists of several bodies connected to each other by means of joints. These joints restrict the system mobility because the motion of different bodies is no longer independent. Consequently, the movement for the bodies in multibody dynamic system are related to each other by means of

constraints equations. Constraints equations can be taken into account in the equations of motion in multibody dynamic system using two techniques; Embedding and Augmented technique. In this study, the kinematic constraint equations are taken into account using augmented technique. Augmented equations of motion formulation are based on the use of Lagrangian multipliers. The kinematic constraint equations can be expressed in the general form as follows:

$$\mathbf{C}(\mathbf{q}, t) = 0 \tag{2.23}$$

where $\mathbf{q}$ is the vector of the total multibody system generalized coordinates, t is the time and $\mathbf{C}$ is the vector of linearly independent constraint equations of the multibody system. The number of degree of freedom (**DOF**) of a multibody system which is equal to the independent generalized coordinates can be expressed as follows:

$$n - n_c = \mathbf{DOF} \tag{2.24}$$

where n is the number of generalized coordinates of the multibody system and n_c is the number of the constraint equations of the system. Applying a virtual displacement to the kinematic constraint equations expressed in **Eq 2.23** leads to the following equation:

$$\mathbf{C_q}\delta\mathbf{q} = 0 \tag{2.25}$$

where $\mathbf{C_q}$ is the jacobian matrix. The jacobian matrix has $(n_c \text{ x } n)$ dimension. Consequently, the jacobian matrix has a full row rank. Jacobian matrix can be obtained by differentiating the algebraic constraint equations with respect to the generalized coordinates of the multibody system. In general it can be expressed as follows:

$$\mathbf{C_q} = \begin{bmatrix} \partial C_1/\partial \mathbf{q}^1 & \partial C_1/\partial \mathbf{q}^2 & \mathsf{L} & \partial C_1/\partial \mathbf{q}^n \\ \partial C_2/\partial \mathbf{q}^1 & \partial C_2/\partial \mathbf{q}^2 & \mathsf{L} & \partial C_2/\partial \mathbf{q}^n \\ \mathsf{M} & \mathsf{M} & \mathsf{M} & \mathsf{M} \\ \partial C_{n_c}/\partial \mathbf{q}^1 & \partial C_{n_c}/\partial \mathbf{q}^2 & \mathsf{L} & \partial C_{n_c}/\partial \mathbf{q}^n \end{bmatrix} \tag{2.26}$$

2.3 Description of Inertia

The mass matrix of the flexible body *i* shown in **Figure 2.1** can be defined using different components as the case in rigid body. The mass matrix can be expressed as follows:

$$\mathbf{M}^i = \begin{bmatrix} \mathbf{m}^i_{RR} & \mathbf{m}^i_{R\theta} & \mathbf{m}^i_{Rf} \\ & \mathbf{m}^i_{\theta\theta} & \mathbf{m}^i_{\theta f} \\ symmetric & & \mathbf{m}^i_{ff} \end{bmatrix} \tag{2.27}$$

where the term $\mathbf{m}^i_{RR}$ represents the mass matrix associated with the translational coordinates of the flexible body *i* coordinate system. It can be expressed as follows:

$$\mathbf{m}^i_{RR} = \int_{V^i} \rho^i \mathbf{I} dV^i = \begin{bmatrix} m^i & 0 \\ 0 & m^i \end{bmatrix} \tag{2.28}$$

where $\mathbf{I}$ is a 2 x 2 identity matrix, ρ^i is the density of the flexible body *i*, V^i is the volume of the flexible body *i* and m^i is the mass of the flexible body *i*. The term $\mathbf{m}^i_{R\theta}$ which represents the coupling between the flexible body *i* reference translational and rotational coordinates can be expressed as follows:

$$\mathbf{m}^i_{R\theta} = \mathbf{A}_\theta \left[\mathbf{I}^i_1 + \overline{\mathbf{S}}^i \mathbf{q}^i_f \right] \tag{2.29}$$

where the vector $\mathbf{I}^i_1$ defines the moment of the body mass about the axes of the body coordinate in the undeformed state. Consequently, the vector $\mathbf{I}^i_1$ will be equal to zero in case the origin of the body coordinate is initially attached to the center of the mass of the body. The vector $\mathbf{I}^i_1$ can be expressed as follows:

$$\mathbf{I}^i_1 = \int_{V^i} \rho^i \overline{\mathbf{u}}^i_o dV^i \tag{2.30}$$

In **Eq 2.29** the vector $\overline{\mathbf{S}}^i \mathbf{q}^i_f$ represents the change in the moment of the mass due to the deformation. In which the matrix $\overline{\mathbf{S}}^i$ can be written as follows:

$$\overline{\mathbf{S}}^i = \int_{V^i} \rho^i \overline{\mathbf{u}}^i_o dV^i \tag{2.31}$$

The term $\mathbf{m}^i_{Rf}$ which represents the coupling between the translational reference motion and the elastic deformation, can be expressed as follows:

$$\mathbf{m}_{Rf}^{i} = \mathbf{A}^{i}\overline{\mathbf{S}}^{i} \tag{2.32}$$

The term $\mathbf{m}_{\theta f}^{i}$ which represents the coupling between the rotational reference motion and the elastic deformation, can be expressed as follows:

$$\mathbf{m}_{\theta f}^{i} = \int_{V^i} \rho^{i}\overline{\mathbf{u}}_{o}^{i}\tilde{\mathbf{I}}\mathbf{S}^{i}dV^{i} + \mathbf{q}_{f}^{iT}\tilde{\mathbf{S}}^{i} \tag{2.33}$$

where $\tilde{\mathbf{I}}$ is a skew symmetric matrix which can be identified as follows:

$$\tilde{\mathbf{I}} = \mathbf{A}_{\theta}^{iT}\mathbf{A}^{i} = \begin{bmatrix} 0 & 1 \\ -1 & 0 \end{bmatrix} \tag{2.34}$$

And $\tilde{\mathbf{S}}^{i}$ is a constant skew symmetric matrix identified as follows:

$$\tilde{\mathbf{S}}^{i} = \int_{V^i} \rho^{i}\mathbf{S}^{iT}\tilde{\mathbf{I}}\mathbf{S}^{i}dV^{i} \tag{2.35}$$

One may note that $\mathbf{m}_{\theta f}^{i}$ consists of two parts; the first part is constant, while the second one depends on the elastic coordinates of the flexible body *i*.

The term $\mathbf{m}_{ff}^{i}$ which is associated with the flexible body *i* coordinates is a constant matrix. The matrix can be defined as follows:

$$\mathbf{m}_{ff}^{i} = \int_{V^i} \rho^{i}\mathbf{S}^{iT}\mathbf{S}^{i}dV^{i} \tag{2.36}$$

The term $\mathbf{m}_{\theta\theta}^{i}$ consists of summation of three scalars identified as follows:

$$\mathbf{m}_{\theta\theta}^{i} = (m_{\theta\theta}^{i})_{rr} + (m_{\theta\theta}^{i})_{rf} + (m_{\theta\theta}^{i})_{ff} \tag{2.37}$$

The first scalar is $(m_{\theta\theta}^{i})_{rr}$ represents the mass moment of inertia of the flexible body *i*, in the undeformed state about perpendicular axis to the plane. It can be identified as follows:

$$(m_{\theta\theta}^{i})_{rr} = \int_{V^i} \rho^{i}\overline{\mathbf{u}}_{o}^{iT}\overline{\mathbf{u}}_{o}^{i}dV^{i} \tag{2.38}$$

The last two scalars $(m_{\theta\theta}^{i})_{rf}$ and $(m_{\theta\theta}^{i})_{ff}$ represent the change in the mass moment of inertia of the flexible body *i* due to deformation. They can be identified respectively as follows:

$$(m_{\theta\theta}^{i})_{rf} = 2\int_{V^i} \rho^{i}\overline{\mathbf{u}}_{o}^{iT}\overline{\mathbf{u}}_{f}^{i}dV^{i} = 2\left[\int_{V^i} \rho^{i}\overline{\mathbf{u}}_{o}^{iT}\mathbf{S}^{i}dV^{i}\right]\mathbf{q}_{f}^{i} \tag{2.39}$$

$$(m_{\theta\theta}^{i})_{ff} = \mathbf{q}_{f}^{iT}\mathbf{m}_{ff}^{i}\mathbf{q}_{f}^{i} \tag{2.40}$$

2.4 Generalized Forces

The generalized forces in the floating frame of reference formulation are divided into two parts; the first part is the generalized external forces, while the second part is the generalized elastic forces. In the **Figure 2.2**, a flexible body *i* is subjected to an external force $\mathbf{F}^i$ acting on an arbitrary point P^i on the body.

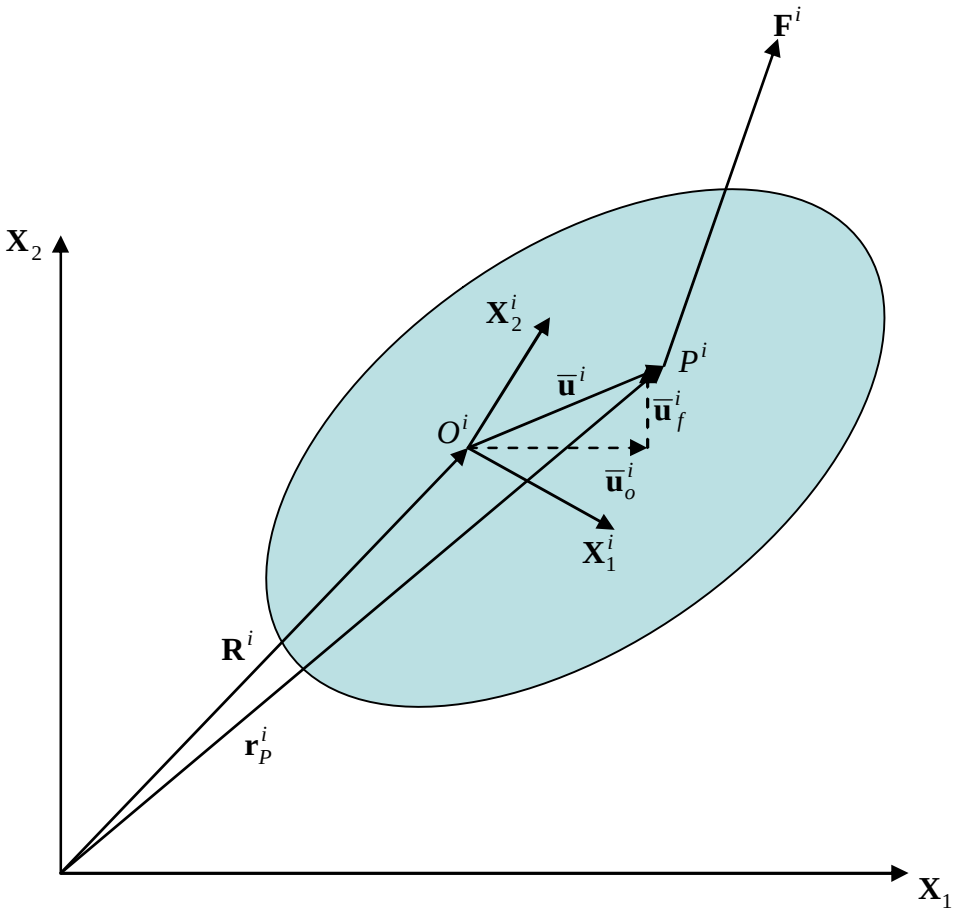

Figure 2.2. Generalized forces in the floating frame of reference formulation.

Generalized External Forces

The vector of an external force $\mathbf{F}^i$ acting on an arbitrary point P^i on the flexible body *i* shown in **Figure 2.2**, can be constant, spring, damping or variable force, or a combination of all them. The virtual work of external forces can be expressed as follows:

$$\delta \mathbf{W}_e^i = \mathbf{Q}_e^i \delta \mathbf{q}^i \tag{2.41}$$

where $\mathbf{Q}_e^i$ is The vector of generalized external forces associated with the generalized coordinates of the flexible body *i*. The vector can be expressed as follows:

$$\mathbf{Q}_e^i = \begin{bmatrix} \mathbf{Q}_R^{iT} & \mathbf{Q}_\theta^{iT} & \mathbf{Q}_f^{iT} \end{bmatrix} \tag{2.42}$$

where $\mathbf{Q}_R^i$ is the vector of generalized external forces associated with the translational reference coordinates of the flexible body *i*. The vector can be expressed as follows:

$$\mathbf{Q}_R^{iT} = \mathbf{F}^{iT} \tag{2.43}$$

The middle component at the middle on the right hand side of **Eq 2.42**, is the vector of generalized external forces associated with the rotational reference coordinate of the flexible body *i*. The vector can be expressed as follows:

$$\mathbf{Q}_\theta^{iT} = \mathbf{F}^{iT} \mathbf{B}^i \tag{2.44}$$

The last component on the right hand side in **Eq 2.42**, is the vector of generalized external forces associated with elastic coordinates of the flexible body *i*. The vector can be expressed as follows:

$$\mathbf{Q}_f^{iT} = \mathbf{F}^{iT} \mathbf{A}^i \mathbf{S}^i \tag{2.45}$$

Generalized Elastic Forces

It is important to note the difference between the virtual work done by the external forces and the elastic forces on the flexible body *i*. It has been noticed previously from **Eq 2.40** that the virtual work done by external force acting on a flexible body *i* is associated with the body generalized coordinates. Consequently, the external force applied to the flexible body *i*, results with a translational or rotational displacement, or both of them, which are associated with reference coordinates of the flexible body *i*. Those types of displacement are called rigid body motion, as the flexibility of the body is not taken into account. In addition the external force applied to the flexible body *i* results with an elastic linear deformation associated with the generalized elastic coordinates of the flexible body *i*. Such deformation affects the shape of the flexible body. It should be mentioned here that this type of deformation due to the body flexibility, may

result with regardless to the existence of external force applied on the body. For example, the elastic deformation of a free rotating beam, when the effect of gravity forces is neglected [17]. The virtual work done by the elastic forces can be expressed as follows:

$$\delta \mathbf{W}_s^i = -\int_{V^i} \boldsymbol{\sigma}^{iT} \delta \boldsymbol{\varepsilon}^i dV^i \tag{2.46}$$

where $\boldsymbol{\sigma}^i$ is the stress vector and $\boldsymbol{\varepsilon}^i$ is the strain vector. The strain vector can be as follows:

$$\boldsymbol{\varepsilon}^i = \mathbf{D}^i \bar{\mathbf{u}}_f^i \tag{2.47}$$

where $\mathbf{D}^i$ is the strain-displacement matrix, which is a matrix whose components are the derivative of the shape functions with respect to the flexible body *i* axes. Substituting **Eq 2.5** into **Eq 2.47**, in order to describe the strain vector in terms of the generalized elastic coordinates of the flexible body *i*, yields to the following equation:

$$\boldsymbol{\varepsilon}^i = \mathbf{D}^i \mathbf{S}^i \mathbf{q}_f^i \tag{2.48}$$

Assuming that the material of the flexible body *i* is a linear isotropic, Hooke's law which relate the stress and strain by the following linear equation can be applied as follows:

$$\boldsymbol{\sigma}^i = \mathbf{E}^i \boldsymbol{\varepsilon}^i \tag{2.49}$$

where $\mathbf{E}^i$ is the symmetric matrix of the elastic coefficients. Substituting **Eq 2.48** into **Eq 2.49** yields to the following equation:

$$\boldsymbol{\sigma}^i = \mathbf{E}^i \mathbf{D}^i \mathbf{S}^i \mathbf{q}_f^i \tag{2.50}$$

Substituting **Eq 2.48** and **Eq 2.50** into **Eq 2.46**, yields to the following equation:

$$\delta \mathbf{W}_s^i = -\int_{V^i} \mathbf{q}_f^{iT} (\mathbf{D}^i \mathbf{S}^i)^T \mathbf{E}^i \mathbf{D}^i \mathbf{S}^i \delta \mathbf{q}_f^i dV^i \tag{2.51}$$

Rearranging the preceding equation, using the symmetrical property of elastic coefficients matrix and the fact that the elastic coordinates of the flexible body *i* depends only on time, yields to the following equation:

$$\delta \mathbf{W}_s^i = -\mathbf{q}_f^{iT} \left[\int_{V^i} (\mathbf{D}^i \mathbf{S}^i)^T \mathbf{E}^i \mathbf{D}^i \mathbf{S}^i dV^i \right] \delta \mathbf{q}_f^i \tag{2.52}$$

The preceding equation can be written as follows:

$$\delta \mathbf{W}_s^i = -\mathbf{q}_f^i \mathbf{K}_{ff}^i \delta \mathbf{q}_f^i \tag{2.53}$$

where $\mathbf{K}_{ff}^i$ is the symmetric positive definite stiffness matrix associated with the generalized elastic coordinates of the flexible body *i*. It can be defined from **Eq 2.52** as follows:

$$\mathbf{K}_{ff}^i = \int_{V^i} (\mathbf{D}^i \mathbf{S}^i)^T \mathbf{E}^i \mathbf{D}^i \mathbf{S}^i dV^i \tag{2.54}$$

The virtual work described in **Eq 2.53** can be written in a partitioned form as follows:

$$\delta \mathbf{W}_s^i = -\begin{bmatrix} \mathbf{R}^{iT} & \theta^{iT} & \mathbf{q}_f^{iT} \end{bmatrix} \begin{bmatrix} 0 & 0 & 0 \\ 0 & 0 & 0 \\ 0 & 0 & \mathbf{K}_{ff}^i \end{bmatrix} \begin{bmatrix} \delta \mathbf{R}^i \\ \delta \theta^i \\ \delta \mathbf{q}_f^i \end{bmatrix} \tag{2.55}$$

One may notice from the previous equation, that the generalized stiffness matrix associated with the generalized coordinates of the flexible body *i* can be defined as follows:

$$\mathbf{K}^i = \begin{bmatrix} 0 & 0 & 0 \\ 0 & 0 & 0 \\ 0 & 0 & \mathbf{K}_{ff}^i \end{bmatrix} \tag{2.56}$$

It is shown clearly from the previous equation that the virtual work of elastic forces due to the flexibility of the body *i*, is associated only with the generalized elastic coordinates of the flexible body *i*.

2.5 Quadratic Velocity Vector

The quadratic velocity vector of the flexible body *i* has three components. The vector can be expressed as follows:

$$\mathbf{Q}_v^i = \begin{bmatrix} (\mathbf{Q}_v^i)_R & (\mathbf{Q}_v^i)_\theta & (\mathbf{Q}_v^i)_f \end{bmatrix}^T \tag{2.57}$$

The first component is associated with the translational reference coordinates of the flexible body *i*. It defines the coriolis and centrifugal forces associated with translational reference coordinates. It can be expressed as follows:

$$(\mathbf{Q}_v^i)_R = (\theta^i)^2 \mathbf{A}^i (\overline{\mathbf{S}}^i \mathbf{q}_f^i + \mathbf{I}_1^i) - 2\dot{\theta}^i \mathbf{A}_\theta^i \overline{\mathbf{S}}^i \dot{\mathbf{q}}_f^i \tag{2.58}$$

The second component is associated with the rotational reference coordinate of the flexible body *i*. It defines the coriolis forces associated with the rotational reference coordinate. It can be identified as follows:

$$(\mathbf{Q}_v^i)_\theta = -2\dot{\theta}^i \dot{\mathbf{q}}_f^{iT} (\mathbf{m}_{ff}^i \mathbf{q}_f^i + \bar{\mathbf{I}}_o^i) \tag{2.59}$$

where $\bar{\mathbf{I}}_o^i$ is identified as follows:

$$\bar{\mathbf{I}}_o^i = \int_{V^i} \rho^i \mathbf{S}^{iT} \bar{\mathbf{u}}_o^i dV^i \tag{2.60}$$

The last component is associated with the elastic coordinates of the flexible body *i*. It defines the centrifugal and coriolis forces associated with the elastic degrees of freedom of the body *i*. It can be expressed as follows:

$$(\mathbf{Q}_v^i)_f = (\dot{\theta}^i)^2 (\mathbf{m}_{ff}^i \mathbf{q}_f^i + \bar{\mathbf{I}}_o^i) + 2\dot{\theta}^i \tilde{\mathbf{S}}^i \dot{\mathbf{q}}_f^i \tag{2.61}$$

2.6 Reference Conditions

In order to define a unique elastic displacement field with respect to the body coordinate system, the flexible body has to be modelled in such a way that the rigid body modes have be eliminated. To this end a set of reference conditions correspond to the selected model have to be applied on the elastic coordinates of the flexible body. The set of the reference conditions has to be chosen carefully as it defines the nature of the flexible body coordinate system [17, 18]. For example, the simply supported and free-free reference conditions define a floating frame body coordinate system, the origin of which is not rigidly attached to a material point of the flexible body beam model. However, the two cantilever beams reference conditions, define a body fixed coordinate system, the origin of which is rigidly attached to the geometric center of the beam in the undeformed state. The reference conditions can be applied by means of a constant matrix called Boolean reference transformation matrix, whose elements are either zeros or ones. The function of this matrix is to select the elastic coordinates, where the reference conditions should be applied. One may notice that **Eq 2.7** includes rigid body modes. Thus, to eliminate those modes, a set of reference conditions have to be applied. In general, **Eq 2.7** can be rewritten after applying the reference conditions as follows:

$$\mathbf{r}_P^i = \mathbf{R}^i + \mathbf{A}^i (\bar{\mathbf{u}}_o^i + \mathbf{S}^i \mathbf{B}_r^i \mathbf{q}_f^i) \tag{2.62}$$

where $\mathbf{B}_r^i$ is the Boolean reference transformation matrix defined by Shabana in Reference [14].

2.7 Equations of Motion

After formulating the mass matrix, the jacobian matrix, the stiffness matrix, the vector of the external generalized forces and the vector of the quadratic velocity, the equations of motion can be formulated using the augmented technique based on using Lagrange multiplies. For a planar flexible body *i* in the multibody dynamic system, Lagrange equation of motion can be expressed as follows:

$$\frac{d}{dt}\left(\frac{\partial T^i}{\partial \dot{\mathbf{q}}^i}\right)^T - \left(\frac{\partial T^i}{\partial \mathbf{q}^i}\right)^T + \mathbf{C}_{\mathbf{q}^i}^T \boldsymbol{\lambda} = \mathbf{Q}^i \tag{2.63}$$

where T^i is the kinetic energy of the flexible body *i*, $\boldsymbol{\lambda}$ is the vector of Lagrange multipliers and $\mathbf{Q}^i$ is the vector of the generalized elastic and external forces. The vector can be expressed as follows:

$$\mathbf{Q}^i = -\mathbf{K}^i \mathbf{q}^i + \mathbf{Q}_e^i \tag{2.64}$$

The first two terms on the left hand side of **Eq 2.63** can be defined as follows:

$$\frac{d}{dt}\left(\frac{\partial T^i}{\partial \dot{\mathbf{q}}^i}\right)^T - \left(\frac{\partial T^i}{\partial \mathbf{q}^i}\right)^T = \mathbf{M}^i \ddot{\mathbf{q}}^i - \mathbf{Q}_v^i \tag{2.65}$$

Substituting **Eq 2.64** and **Eq 2.65** into **Eq 2.63** yields to the following Lagrange equation of motion:

$$\mathbf{M}^i \ddot{\mathbf{q}}^i + \mathbf{K}^i \mathbf{q}^i + \mathbf{C}_{\mathbf{q}^i}^T \boldsymbol{\lambda} = \mathbf{Q}_e^i + \mathbf{Q}_v^i \qquad i = 1,2,...n_b \tag{2.66}$$

where n_b is the total number of the bodies in the planar multibody dynamic system. The previous equation can be expressed in a partitioned form as follows:

$$\begin{bmatrix} \mathbf{m}_{RR}^I & \mathbf{m}_{R\theta}^i & \mathbf{m}_{Rf}^i \\ \mathbf{0} & \mathbf{m}_{\theta\theta}^i & \mathbf{m}_{\theta f}^i \\ symmetric & & \mathbf{m}_{ff}^i \end{bmatrix} \begin{bmatrix} \ddot{\mathbf{R}}^i \\ \ddot{\theta}^i \\ \ddot{\mathbf{q}}_f^i \end{bmatrix} + \begin{bmatrix} 0 & 0 & 0 \\ 0 & 0 & 0 \\ 0 & 0 & \mathbf{K}_{ff}^i \end{bmatrix} \begin{bmatrix} \mathbf{R}^i \\ \theta^i \\ \mathbf{q}_f^i \end{bmatrix} + \begin{bmatrix} \mathbf{C}_{\mathbf{R}^i}^T \\ \mathbf{C}_{\theta^i}^T \\ \mathbf{C}_{\mathbf{q}_f^i}^T \end{bmatrix} \boldsymbol{\lambda} \tag{2.67}$$

$$= \begin{bmatrix} (\mathbf{Q}_e^i)_R \\ (\mathbf{Q}_e^i)_\theta \\ (\mathbf{Q}_e^i)_f \end{bmatrix} + \begin{bmatrix} (\mathbf{Q}_v^i)_R \\ (\mathbf{Q}_v^i)_\theta \\ (\mathbf{Q}_v^i)_f \end{bmatrix}$$

Equation **2.66** is a system of second order differential equations that has $(n+n_c)$ number of unknowns while the number of equations is *n*. Therefore, additional kinematic constraint algebraic equations describing the joints between the bodies in the system are added. Those equations have to be satisfied at all times during the motion. The addition of those constraint equations leads to the following set of **DAE**:

$$\mathbf{M}^i\ddot{\mathbf{q}}^i + \mathbf{K}^i\mathbf{q}^i + \mathbf{C}_{\mathbf{q}^i}^T\boldsymbol{\lambda} = \mathbf{Q}_e^i + \mathbf{Q}_v^i \qquad i = 1,2,...,n_b \tag{2.68}$$

$$\mathbf{C}(\mathbf{q}^i, t) = \mathbf{0}$$

2.8 Finite Element Assembling Procedure

Finite element procedure is used in the floating frame of reference formulation to describe the elastic deformation of the flexible body with increased accuracy. Moreover, exact modelling of rigid body motion associated with large translation and rotation can be obtained, while infinitesimal rotations are used as nodal coordinates. In the finite element floating frame of reference, the flexible body is discretized to a finite number of elements. Each element consists of number of nodes results from discretization, which defines the elastic deformation of the element. The position of each element is defined with respect to the body coordinate system using element coordinate system. The elastic deformation of each element is defined using nodal coordinates and space dependant element shape matrix. The nodal coordinates for each element are identified in terms of the total nodal coordinates of the flexible body using Boolean transformation matrix. Reference conditions are applied at the boundary nodes of the flexible body in order to eliminate the rigid body modes. For more convenience, **Figure 2.3** shows the coordinate systems for a planar flexible body *i* in finite element floating frame of reference.

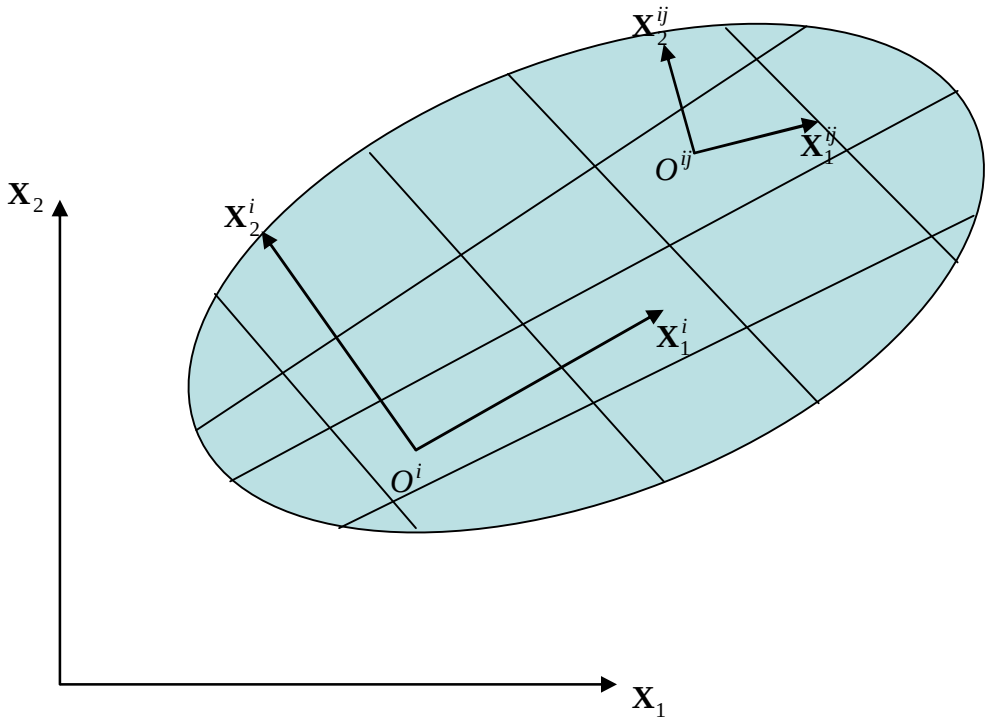

Figure 2.3. Finite element floating frame of reference coordinates.

It can be noticed from **Figure 2.3** that the flexible body *i* has been discretized to a finite number of elements. The origin O^{ij} of the element *j* coordinate system $\mathbf{X}_1^{ij}\mathbf{X}_2^{ij}$ is rigidly attached to a point on the element. While on the other hand, the origin O^{i} of the flexible body *i* coordinate system $\mathbf{X}_1^{i}\mathbf{X}_2^{i}$ is not necessarily has to be rigidly attached to a point on the flexible body. All the positions of the elements have to be defined with respect to the body coordinate system. Therefore, it serves as a reference for all elements and expresses the connectivity between them. The orientation of the flexible body *i* coordinate system is defined with respect to the global coordinate system using the transformation matrix defined in **Eq 2.8**. In the finite element floating frame of reference assembling procedure two constant mapping matrices are needed to be identified. Those matrices do not change and are kept constant during the simulation. The first matrix is a 2 x 2 transformation matrix used to define the orientation of the element *j* coordinate system with respect to the flexible body *i* coordinate system. The matrix can be expressed as follows:

$$\mathbf{C}^{ij} = \begin{bmatrix} \cos\beta^{ij} & -\sin\beta^{ij} \\ \sin\beta^{ij} & \cos\beta^{ij} \end{bmatrix} \tag{2.69}$$

where the subscript ij refers to the element j in the flexible body i and β^{ij} is the orientation angle of the element j coordinate system with respect to the flexible body i coordinate system. The second matrix is called Boolean mapping transformation matrix, whose elements are either zeros or ones. This matrix is used to define the vector of element ij nodal coordinates in terms of the total vector of elastic nodal coordinates of the flexible body i as follows:

$$\mathbf{e}^{ij} = \mathbf{B}^{ij}\mathbf{e}^{iT} \tag{2.70}$$

where $\mathbf{e}^{ij}$ is the vector of the element ij nodal coordinates, $\mathbf{B}^{ij}$ is the Boolean mapping transformation matrix which is defined by Shabana in Reference [14] and $\mathbf{e}^{i}$ is the vector of the total elastic nodal coordinates of the flexible body i. Recalling **Eq 2.70** the vector of nodal coordinates of the element ij can be expressed as follows:

$$\mathbf{e}^{ij} = \mathbf{e}_o^{ij} + \mathbf{e}_f^{ij} \tag{2.71}$$

where $\mathbf{e}_o^{ij}$ defines the nodal coordinates of the element ij in the undeformed state and $\mathbf{e}_f^{ij}$ defines the elastic deformation of the nodal coordinates of the element ij. The assumed displacement field of the nodal coordinates of the element ij can be expressed in the element ij coordinate system using the shape function of the element ij as follows:

$$\mathbf{w}^{ij} = \mathbf{S}^{ij}\mathbf{e}^{ij} \tag{2.72}$$

where $\mathbf{S}^{ij}$ is the space dependant shape matrix of the element ij. The assumed displacement field of the nodal coordinates of the element ij defined in the previous equation can be expressed with respect to the flexible body i coordinate system as follows:

$$\bar{\mathbf{u}}^{ij} = \mathbf{C}^{ij}\mathbf{w}^{ij} \tag{2.73}$$

where $\bar{\mathbf{u}}^{ij}$ is the vector of the assumed displacement field of the nodal coordinates of the element ij defined with respect to the flexible body i coordinate system. Substituting **Eq 2.72** and **Eq 2.70** into **Eq 2.73** yields to the following equation:

$$\bar{\mathbf{u}}^{ij} = \mathbf{C}^{ij}\mathbf{S}^{ij}\mathbf{B}^{ij}\mathbf{e}^{iT} \tag{2.74}$$

The preceding equation can be written in a more compact form as follows:

$$\bar{\mathbf{u}}^{ij} = \mathbf{N}^{ij}\mathbf{e}^{iT} \tag{2.75}$$

where $\mathbf{N}^{ij}$ can be described from **Eq 2.74** as follows:

$$\mathbf{N}^{ij} = \mathbf{C}^{ij}\mathbf{S}^{ij}\mathbf{B}^{ij} \tag{2.76}$$

The vector describes the position of any arbitrary point P^{ij} on the element *ij* can be expressed with respect to the global coordinate system using the two constant mapping matrices as follows:

$$\mathbf{r}_P^{ij} = \mathbf{R}^i + \mathbf{A}^i\mathbf{N}^{ij}\mathbf{e}^i \tag{2.77}$$

where $\mathbf{r}_P^{ij}$ is the vector describes the location for any arbitrary point P^{ij} on the element *ij* with respect to the global coordinate system.

2.9 Modal Reduction

Using finite element method in the floating frame of reference formulation results with a large number of generalized elastic nodal coordinates of the flexible body. This is due to the flexible body discretization into finite number of elements which leads to a large number of nodal degrees of freedom. Thus, describing the deformation of the body, requires describing the deformation for each node, which leads to a long and expensive computation. As a result, a modal reduction method can be adopted to reduce the generalized elastic nodal coordinates. The reduction is achieved by eliminating the high natural frequency modes which may carry little energy. Removing those types of vibration modes associated with high natural frequencies prevent the body from adopting the particular deformation shape associated with this mode. Vibration modes with high natural frequencies have deformation shape, which are not important and interesting in practice, so eliminating them will not affect considerably the solution. Modal reduction offers an efficient way to reduce the number of generalized elastic nodal coordinates with a minimum effect in accuracy of the solution. Modal reduction can be carried out by transferring from the physical nodal coordinate system of the deformable body into the modal elastic coordinates. This can be accomplished by modal transformation. Modal transformation can be adopted using the following two steps. First step, is to solve the eigenvalue equation derived by assuming the

flexible body *i* vibrating freely about a reference configuration. The equation is defined as follows:

$$\mathbf{m}^i_{ff}\ddot{\mathbf{e}}^i + \mathbf{K}^i_{ff}\mathbf{e}^i = \mathbf{0} \tag{2.78}$$

where $\ddot{\mathbf{e}}^i$ is the acceleration of the elastic nodal coordinates of the flexible body *i*. A trial solution for the preceding equation which has been suggested by (Clough and Penzien 1975; Shabana 1997) can be defined as follows:

$$\mathbf{e}^i = \mathbf{a}^i e^{j\omega t} \tag{2.79}$$

Substituting the preceding equation into **Eq 2.78** yields to the following equation:

$$\left[\mathbf{K}^i_{ff} - (\omega^i_k)^2 \mathbf{m}^i_{ff}\right] \mathbf{a}^i_k = \mathbf{0} \qquad k = 1,2,...,n_n \tag{2.80}$$

The preceding equation is called the standard eigenvalue problem. Where n_n is the number of the elastic nodal coordinates of the flexible body *i* resulted from discretization, ω^i_k is a set of eigenvalues or natural frequencies associated with each nodal coordinate of the flexible body *i* and $\mathbf{a}^i_k$ are the corresponding eigenvectors for the eigenvalues. The eigenvectors are sometimes called as the normal modes or the mode shapes. The second step is to eliminate the modes associated with high natural frequencies, in addition to the rigid boy modes. The modes that have zero natural frequencies and thus zero eigenvalues are called rigid body modes. As a result of the second step, a reduced model with m low frequency mode shapes can be obtained. It is important to note that the number of mode shapes results after elimination m is much less than the number of the nodal coordinates n_n $(m << n_n)$. After choosing the mode shapes best describing the deformation of the body *i*, a coordinate transformation from the physical nodal coordinates to the modal elastic nodal coordinates can be accomplished as follows:

$$\mathbf{e}^i \approx \overline{\mathbf{\Phi}}^i \mathbf{p}^i_f \tag{2.81}$$

where $\mathbf{p}^i_f$ is the vector of the modal elastic nodal coordinates of the flexible body *i* and $\overline{\mathbf{\Phi}}^i$ is the modal transformation matrix whose columns are the low frequency m mode shapes. The matrix can be expressed as follows:

$$\overline{\mathbf{\Phi}}^i = \left[\mathbf{a}^i_1 \quad \mathbf{a}^i_2 \quad \cdots \quad \mathbf{a}^i_m\right] \tag{2.82}$$

where $\mathbf{a}_m^i$ represents the mode shape correspond to the low natural frequency ω_m^i. The vector of the generalized coordinates system of the flexible body *i* can be expressed by means of the modal coordinate system as follows:

$$\mathbf{q}^i \approx \mathbf{\Phi}^i \mathbf{p}^i \tag{2.83}$$

where $\mathbf{p}^i$ is the vector of the modal coordinates of the flexible body *i* and $\mathbf{\Phi}^i$ is the modal transformation matrix for the total vector of the generalized coordinates system of the flexible body *i*. The preceding equation can be rewritten in a partitioned form as follows:

$$\begin{bmatrix} \mathbf{q}_r^i \\ \mathbf{e}^i \end{bmatrix} = \begin{bmatrix} \mathbf{I} & \mathbf{0} \\ \mathbf{0} & \overline{\mathbf{\Phi}}^i \end{bmatrix} \begin{bmatrix} \mathbf{p}_r^i \\ \mathbf{p}_f^i \end{bmatrix} \tag{2.84}$$

where $\mathbf{p}_r^i$ is the vector of the modal reference coordinates. It can be noticed from the previous equation that the reference modal coordinates are equal to the physical reference coordinates.

Orthogonality of the Mode Shapes

The orthogonality of the mode shapes which was proven by Shabana [15], is an important property. This property can be used to obtain a diagonal mass and stiffness matrices which yield to m_d number of uncoupled differential equations. To this end, **Eq 2.68** can be rewritten using the vector of the modal coordinates of the flexible body *i* as follows:

$$\mathbf{M}^i \mathbf{\Phi}^i \ddot{\mathbf{p}}^i + \mathbf{K}^i \mathbf{\Phi}^i \mathbf{p}^i + \mathbf{C}_{\mathbf{p}^i}^T \boldsymbol{\lambda} = \mathbf{Q}_e^i + \mathbf{Q}_v^i \tag{2.85}$$

Premultiplying the preceding equation by $\mathbf{\Phi}^{iT}$ yields to the following equation:

$$\mathbf{\Phi}^{iT} \mathbf{M}^i \mathbf{\Phi}^i \ddot{\mathbf{p}}^i + \mathbf{\Phi}^{iT} \mathbf{K}^i \mathbf{\Phi}^i \mathbf{p}^i + \mathbf{\Phi}^{iT} \mathbf{C}_{\mathbf{p}^i}^T \boldsymbol{\lambda} = \overline{\mathbf{Q}}_e^i + \overline{\mathbf{Q}}_v^i \tag{2.86}$$

where $\mathbf{\Phi}^{iT} \mathbf{M}^i \mathbf{\Phi}^i$ can be expressed as follows:

$$\mathbf{M}_p^i = \mathbf{\Phi}^{iT} \mathbf{M}^i \mathbf{\Phi}^i = \begin{bmatrix} \mathbf{a}_1^{iT} \mathbf{M}^i \mathbf{a}_1^{iT} & 0 & 0 & 0 \\ 0 & \mathbf{a}_2^{iT} \mathbf{M}^i \mathbf{a}_2^{iT} & 0 & 0 \\ \mathbb{M} & \mathbb{M} & \mathbb{O} & \mathbb{M} \\ 0 & 0 & 0 & \mathbf{a}_m^{iT} \mathbf{M}^i \mathbf{a}_m^{iT} \end{bmatrix} \tag{2.87}$$

$$= \begin{bmatrix} \hat{m}_1^i & 0 & 0 & 0 \\ 0 & \hat{m}_2^i & 0 & 0 \\ \mathbb{M} & \mathbb{M} & \mathbb{O} & \mathbb{M} \\ 0 & 0 & 0 & \hat{m}_m^i \end{bmatrix}$$

where $\mathbf{M}_p^i$ is the modal mass matrix and $\hat{m}^i$ are the modal mass coefficients. The matrix $\mathbf{\Phi}^{iT}\mathbf{K}^i\mathbf{\Phi}^i$ can be expressed as follows:

$$\mathbf{K}_p^i = \mathbf{\Phi}^{iT}\mathbf{K}^i\mathbf{\Phi}^i = \begin{bmatrix} \mathbf{a}_1^{iT}\mathbf{K}^i\mathbf{a}_1^{iT} & 0 & 0 & 0 \\ 0 & \mathbf{a}_2^{iT}\mathbf{K}^i\mathbf{a}_2^{iT} & 0 & 0 \\ \mathbb{M} & \mathbb{M} & \mathbb{O} & \mathbb{M} \\ 0 & 0 & 0 & \mathbf{a}_m^{iT}\mathbf{K}^i\mathbf{a}_m^{iT} \end{bmatrix} \tag{2.88}$$

$$= \begin{bmatrix} k_1^i & 0 & 0 & 0 \\ 0 & k_2^i & 0 & 0 \\ \mathbb{M} & & \mathbb{O} & \mathbb{M} \\ 0 & 0 & 0 & k_m^i \end{bmatrix}$$

where $\mathbf{K}_p^i$ is called the modal stiffness matrix and k^i are the modal stiffness coefficients. It can be noticed from **Eq 2.87** and **Eq 2.88** that the modal mass and stiffness matrices are diagonal as a result of the orthogonality property of the mode shapes. The vectors on the right hand side of the **Eq 2.86** can be expressed respectively as follows:

$$\overline{\mathbf{Q}}_e^i = \mathbf{\Phi}^{iT}\mathbf{Q}_e^i \tag{2.89}$$

$$\overline{\mathbf{Q}}_v^i = \mathbf{\Phi}^{iT}\mathbf{Q}_v^i \tag{2.90}$$

It is important to note from **Eq 2.86** that the jacobian matrix is evaluated by differentiating the constraint equations with respect to the modal coordinates. However, it is more convenient to differentiate the constraint equations with respect to the physical coordinates. This can be accomplished using the following relation:

$$\mathbf{C}_{\mathbf{p}^i} = \frac{\partial \mathbf{C}}{\partial \mathbf{p}^i} = \frac{\partial \mathbf{C}}{\partial \mathbf{q}^i}\frac{\partial \mathbf{q}^i}{\partial \mathbf{p}^i} = \mathbf{C}_{\mathbf{p}^i}\mathbf{\Phi}^i \tag{2.91}$$

Therefore the jacobian matrices associated with the modal reference and elastic nodal coordinates can be expressed as follows:

$$\mathbf{C}_{\mathbf{p}_r^i} = \mathbf{C}_{\mathbf{q}_r^i} \tag{2.92}$$

$$\mathbf{C}_{\mathbf{p}_f^i} = \mathbf{C}_{\mathbf{e}^i} \overline{\mathbf{\Phi}}^i \tag{2.93}$$

Solving **Eq 2.86** yields to a number *m* of modal elastic nodal coordinates. Substituting the solution into **Eq 2.81** yields to the physical elastic nodal coordinates which describe the deformation of the body *i*.

Craig-Bampton Method

The modal transformation matrix expressed in **Eq 2.82** contains the selected mode shapes that best describe the deformation. However, to obtain acceptable dynamic accuracy, an excessive number of mode shapes may be still required. As a result, the modal reduction may lose its importance in decreasing the number of deformation mode shapes which are not interesting. To overcome this problem, one of the component mode synthesis (**CMS**) methods, which has been widely used and is available in a number of commercial finite element codes such as **ANSYS** [19] can be applied. This method is called Craig-Bampton method [20]. This method can be applied by defining two sets of modes known as Craig-Bampton modes. The first set is called constraint modes, which can be obtained by giving each boundary **DOF** a unit displacement while holding all other boundary **DOF** fixed. These modes span all possible motions of the boundary **DOF**. To illustrate the methodology of the constraint modes, **Figure 2.4** shows an example of two different constraint modes for a beam that has attachment points at the two ends.

Figure 2.4. Craig-Bampton constraint modes.

The previous figure on the left, shows the constraint mode corresponds to a unit translation, while the figure on the right, shows the constraint mode corresponds to a unit rotation. The second set is called fixed boundary normal modes, which can be obtained by fixing the boundary **DOF** and computing an eigensolution. These modes span all possible motions of the interior **DOF**. To illustrate the

methodology of the fixed boundary normal modes, **Figure 2.5** shows two different fixed boundary normal modes for a beam that has attachment points at the two ends.

Figure 2.5. Craig-Bampton fixed boundary normal modes.

As a result of defining the previous two sets of modes, a new set of coordinates, called modal coordinates of the Craig-Bampton modes, is formed. Modal coordinates of the Craig-Bampton modes can be defined by means of the vector of generalized coordinates system of the flexible body *i* as follows:

$$\mathbf{q}^i = \boldsymbol{\Psi}^i \hat{\mathbf{p}}^i \tag{2.94}$$

where $\boldsymbol{\Psi}^i$ is the Craig-Bampton transformation matrix of the vector of generalized coordinates system of the flexible body *i* and $\hat{\mathbf{p}}^i$ is the vector of modal coordinates of the Craig-Bampton modes. The preceding equation can be rewritten in a more explicit form as follows:

$$\begin{bmatrix} \mathbf{q}_r^i \\ \mathbf{e}^i \end{bmatrix} = \begin{bmatrix} \mathbf{I} & \mathbf{0} \\ \boldsymbol{\Psi}_{IC}^i & \boldsymbol{\Psi}_{IN}^i \end{bmatrix} \begin{bmatrix} \hat{\mathbf{p}}_C^i \\ \hat{\mathbf{p}}_N^i \end{bmatrix} \tag{2.95}$$

where $\boldsymbol{\Psi}_{IC}^i$ is the Craig-Bampton transformation matrix of the vector of elastic nodal coordinates of the flexible body *i* or the ineterior **DOF** in the constraint modes, $\boldsymbol{\Psi}_{IN}^i$ is the Craig-Bampton transformation matrix of the vector of elastic nodal coordinates of the flexible body *i* or the ineterior **DOF** in the normal modes, $\hat{\mathbf{p}}_C^i$ is the vector of modal coordinates of the Craig-Bampton constraint modes of the flexible body *i* and $\hat{\mathbf{p}}_N^i$ is the vector of modal coordinates of the Craig-Bampton fixed boundary normal modes of the flexible body *i*. The Craig-Bampton modes are not orthogonal. Therefore, the Craig-Bampton transformation matrix is unsuitable for direct use in dynamic system simulation, as it can not be

utilized to obtain diagonal mass and stiffness matrices. To overcome this problem, a new transformation matrix $\hat{\mathbf{N}}^i$ which transforms the Craig-Bampton modes to equivalent orthogonal modes expressed by means of modal coordinates is defined. The new transformation matrix can be obtained by solving the following eigenvalue problem:

$$\left[\hat{\mathbf{K}}^i - (\lambda^i)^2 \hat{\mathbf{M}}^i\right] \boldsymbol{\Omega}^i = \mathbf{0} \tag{2.96}$$

where $\hat{\mathbf{K}}^i$ is the Craig-Bampton stiffness transformation matrix, which can be expressed by means of the generalized stiffness matrix of the flexible body *i* as follows:

$$\hat{\mathbf{K}}^i = \boldsymbol{\Psi}^{iT} \mathbf{K}^i \boldsymbol{\Psi}^i \tag{2.97}$$

λ^i in **Eq 2.96** is a set of eigenvalues or natural frequencies associated with each modal coordinate of the Craig-Bampton modes of the flexible body *i*, $\boldsymbol{\Omega}^i$ are the corresponding orthogonal eigenvectors for the eigenvalues and $\hat{\mathbf{M}}^i$ is the Craig-Bampton mass transformation matrix, which can be expressed by means of the generalized mass matrix of the flexible body *i* as follows:

$$\hat{\mathbf{M}}^i = \boldsymbol{\Psi}^{iT} \mathbf{M}^i \boldsymbol{\Psi}^i \tag{2.98}$$

The orthogonal eigenvectors $\boldsymbol{\Omega}^i$ result from solving the eigenvalue problem expressed in **Eq 2.96** are arranged in the transformation matrix $\hat{\mathbf{N}}^i$, which transforms the modal coordinates of the Craig-Bampton modes to an equivalent orthogonal modal coordinates. Consequently, the modal coordinates can be expressed by means of modal coordinates of the Craig-Bampton modes as follows:

$$\mathbf{p}^i = \hat{\mathbf{N}}^i \hat{\mathbf{p}}^i \tag{2.99}$$

Using **Eq 2.83** and **Eq 2.99** the effect of the superposition can be expressed as follows:

$$\mathbf{q}^i = \boldsymbol{\Phi}^i \mathbf{p}^i = \boldsymbol{\Phi}^i \hat{\mathbf{N}}^i \hat{\mathbf{p}}^i \tag{2.100}$$

The Craig-Bampton transformation matrix of the vector of generalized coordinates system of the flexible body *i* can be expressed using the previous equation as follows:

$$\boldsymbol{\Psi}^i = \boldsymbol{\Phi}^i \hat{\mathbf{N}}^i \tag{2.101}$$

3. SIMULATION MODEL OF THE HUMAN LOWER LIMB

In this chapter, the procedure of building a two dimensional human lower limb simulation model is shown. For the sake of simplicity, the model is assumed to be consisting of three bodies or bones; the thigh, the shank and the foot, which they were shown previously in **Figure 1.2**. The shank bone only is modeled as a flexible body. While on the other hand, the thigh and the foot bones are modeled as rigid bodies. The model consists of three revolute joints; first one connects the foot and the shank, second one connects the shank and the thigh and the third one connects the thigh and the human skeleton. In this work, **MCS.ADAMS** software [21] version 12.0 is used to study and analyze the lower limb model. Moreover, the software is used to calculate the strain in the shank bone as a result of applying different exercises to this model. In the following chapter, raising the sole of the foot is considered the exercise to be applied to the lower limb model.

The geometrical model of the lower limb has been built based on the Visible Human Viewer Project [22]. The visible human project is a Java Applet written to allow users to explore slices of the visible human data set from three different viewpoints (axial, coronal, and sagittal). It is the creation of complete, anatomically detailed, three-dimensional representations of the normal male and female human bodies. Acquisition of transverse computerized tomography (**CT**), magnetic resonance imaging (**MRI**) and cryosection images of representative male and female cadavers has been completed. The male was sectioned at one millimeter intervals, the female at one-third of a millimeter intervals. The visible man is a set of digital images of the body of a 39 year old man, Joseph Paul Jernigan, who donated his body to science after being convicted of murder and sentenced to death. He was executed by lethal injection in Texas in 1993. The visible man data was made available in 1994. The visible woman data is for a 59 year old woman who died of natural causes. This data was made available in December 1995. In this model, the lower limb of the male is only considered. **Figure 3.1** shows the main panel of the applet which contains the preview three images (axial, coronal, and sagittal) of the human body.

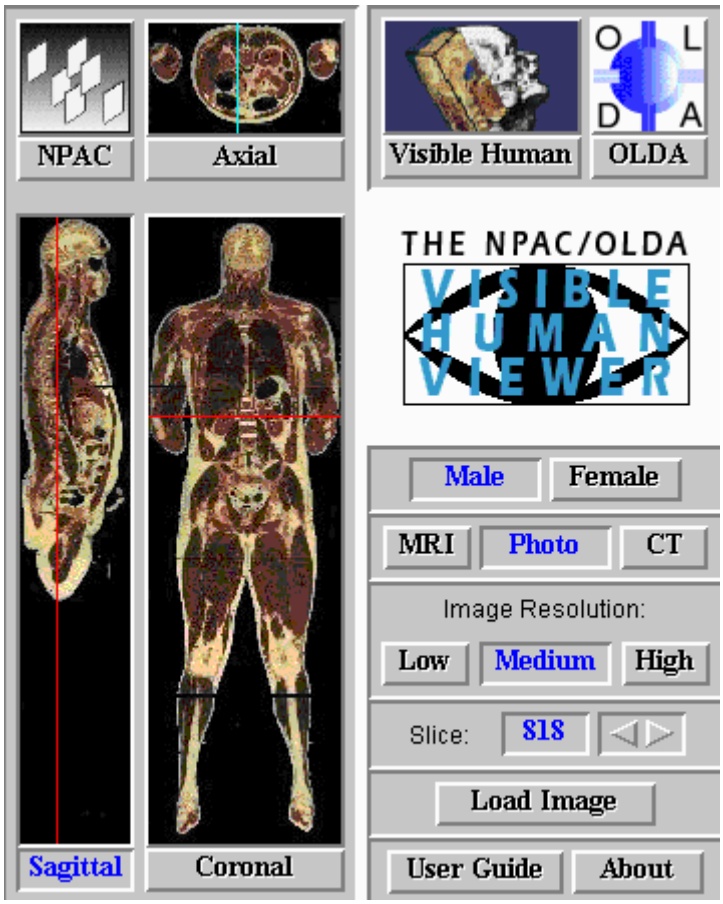

Figure 3.1. Visible human viewer main panel [22].

It can be noticed from **Figure 3.1** that in addition to the three viewpoints shown in the main panel, a control panel is also included in the main panel that provides several options to the user. Through the control panel, the user can select the image type (male or female), the image format (**MRI**, Photo or **CT**), the image resolution (Low, Medium or High), the image to be magnified (Load Image) and the image to be previewed through the slice adjust triangular buttons that moves the cutting line on each viewpoint image. Since the male viewpoint images were sectioned to one millimeter intervals, the slices triangular buttons can be used for measuring purposes.

3.1 Shank Model

The shank bone has two parts; the anterior and the posterior. The two parts are connected together at their endings, and they have complicated geometrical features. **Figure 3.2** shows the geometrical shape of the male shank bone as well

as the cross section at the middle point of it, as depicted from the visible human viewer.

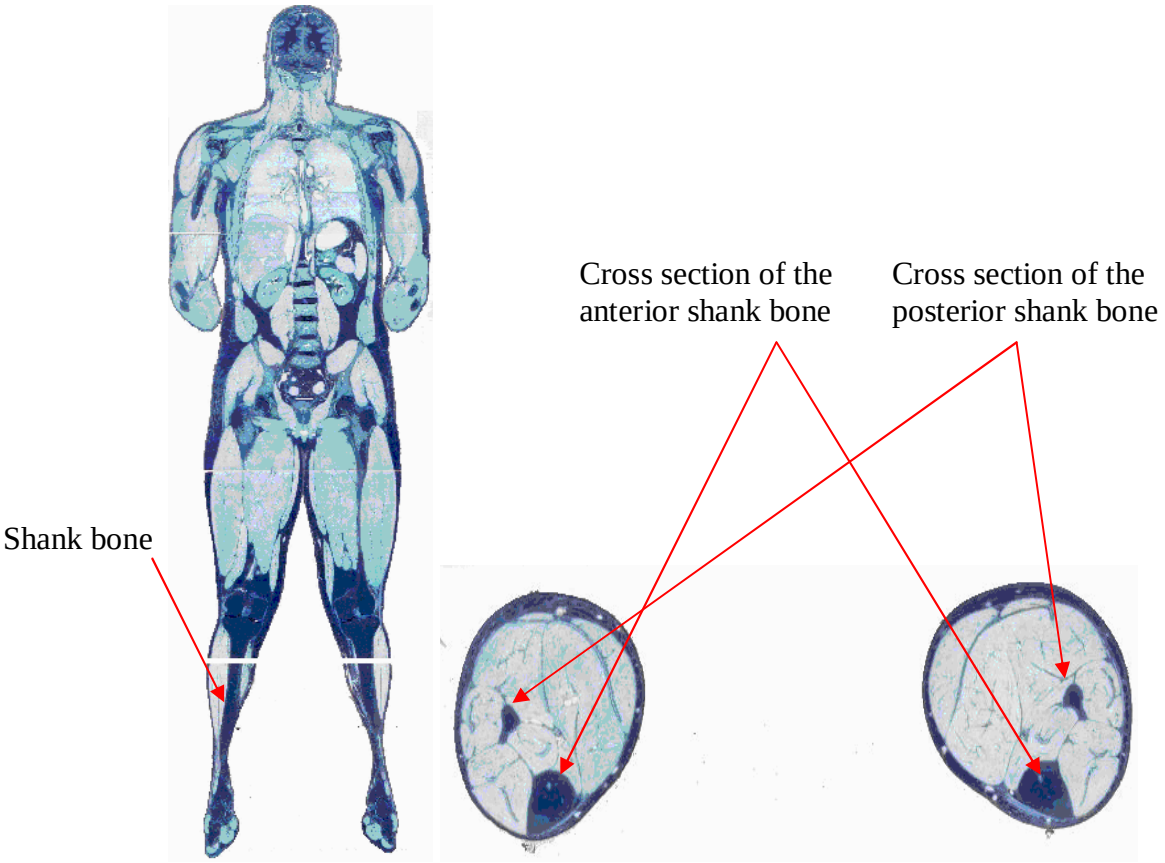

Figure 3.2. Geometrical shape and cross section of the shank bone [22].

It can be noticed from **Figure 3.2** that the geometrical shape and the cross section of the anterior and posterior shank bone have irregular shapes. For simplicity, the shank is modeled as one body, the cross section is assumed to be hollow circular and the shape of the two endings of the shank bone is assumed to be identical at each end. **Table 3.1** shows the dimensions used to build the shank bone model in addition to other physical specifications needed. The model of the shank bone is shown in **Figure 3.3**.

Table 3.1. Dimensions and specifications of the shank bone model.

Parameters	**Values**
Length	0.421 m
Outer radius	0.037 m
Inner radius	0.027 m
Mass	3 kg
Center of gravity location as a percentage of the shank length measured from the proximal end	43.4 %
Elastic modulus	17 GPa

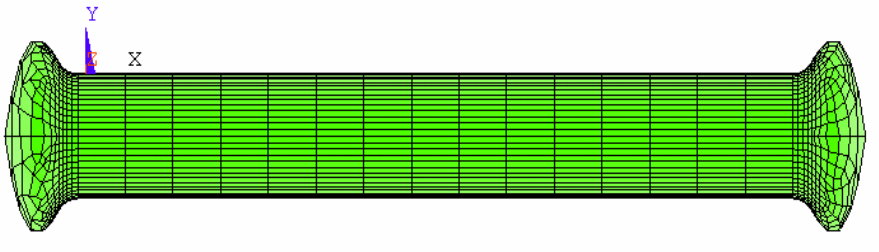

Figure 3.3. Shank bone model.

The model shown in the previous figure is built using **ANSYS 8.1** software. The bone is meshed using shell element with type *shell 63*. **ANSYS** software is used to calculate the number of the deformation mode shapes needed in the floating frame of reference formulation based on the Craig-Bampton method explained in chapter two.

Deformation Mode Shapes

The number of deformation modes, in addition to the strain and stress results associated with each deformation mode can be calculated and transferred to **ADAMS** software. The deformation mode shapes can be investigated and analyzed through **ADAMS** software in which the user has the option to select the suitable deformation modes. Usually the first six modes represent the rigid body modes, where the natural frequency associated with them are $\approx$zero. By default, the rigid body modes are automatically disabled through the software, however, the user has to check carefully the other transferred modes in order to disable the unsuitable deformation modes. **Figure 3.5** shows the selected elastic deformation mode shapes of the shank bone model, and **Table 3.2** shows the natural frequencies associated with each mode.

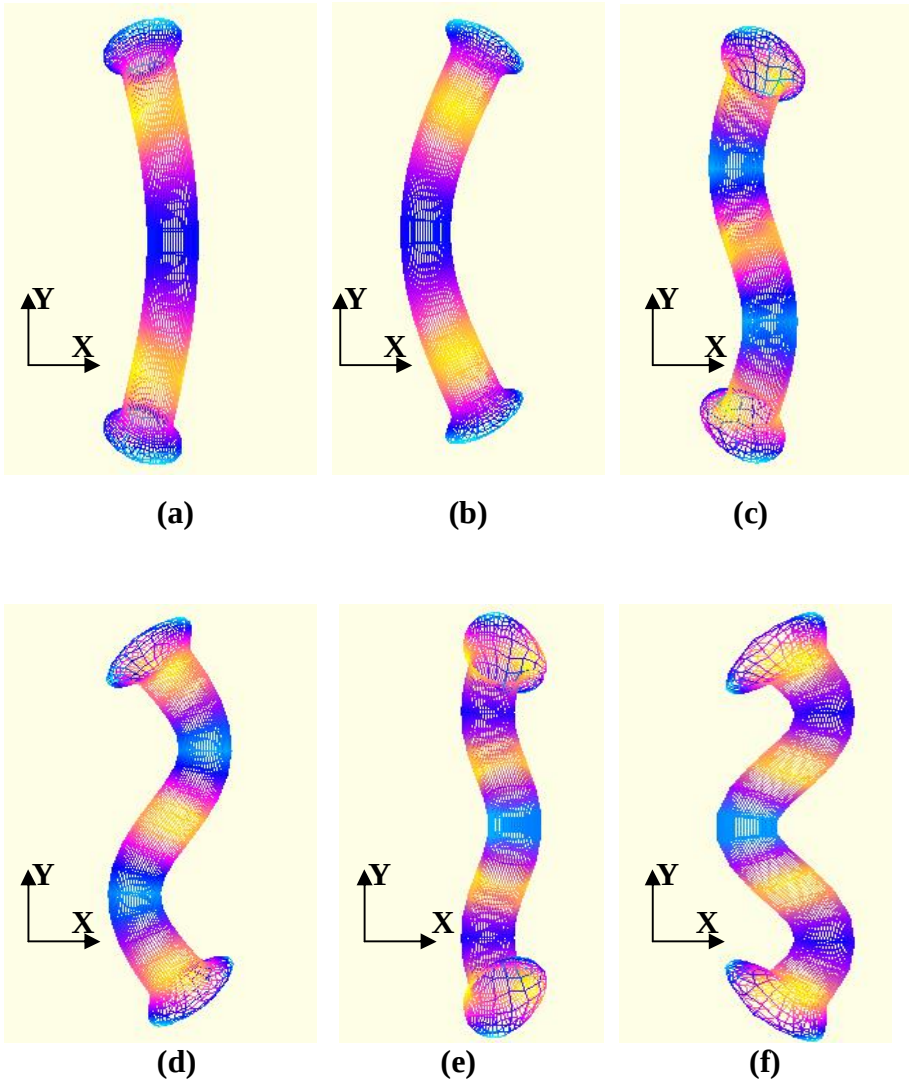

Figure 3.4. Selected elastic deformation modes for the shank bone.

Table 3.2. Natural frequencies of the selected deformation modes.

Deformation Mode	**Natural Frequency (Hz)**
(a)	652.054
(b)	652.117
(c)	1596.295
(d)	1596.664
(e)	2634.429
(f)	2635.569

3.2 Thigh Model

Similar to the shank bone, the thigh bone has complicated geometrical features as well. **Figure 3.5** shows the geometrical shape of the male thigh bone as well as the cross section at the middle point of it, as depicted from the visible human viewer.

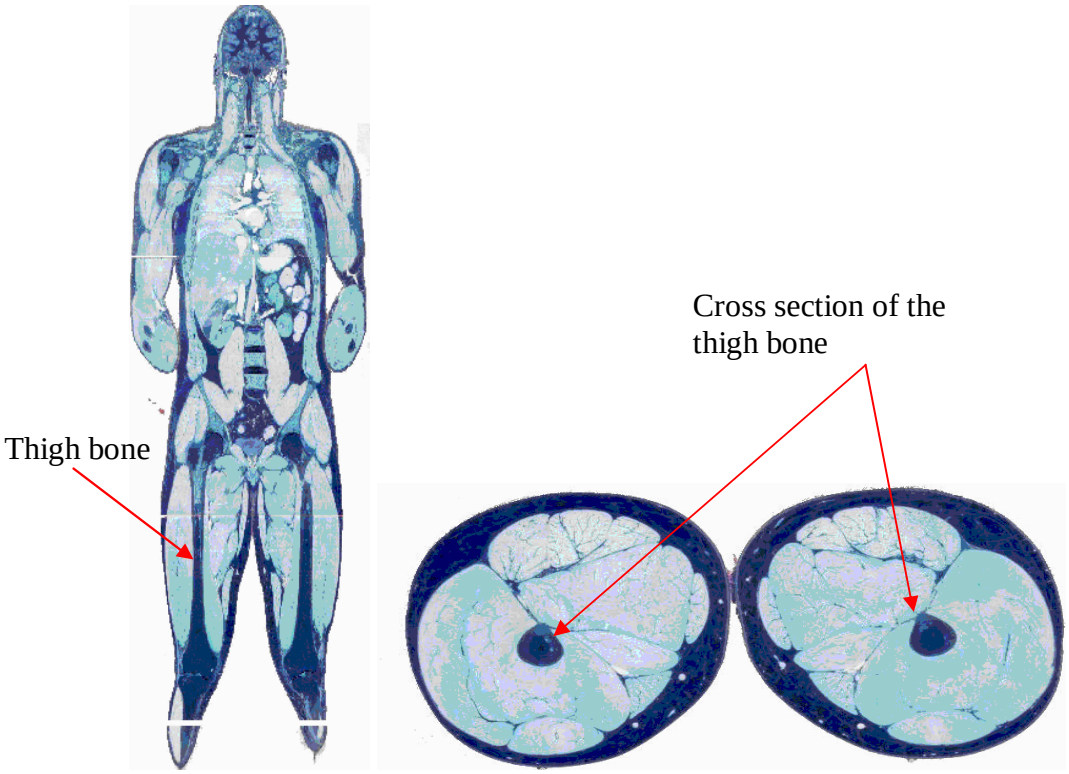

Figure 3.5. Geometrical shape and cross section of the thigh bone [22].

It can be noticed from **Figure 3.5** that the geometrical shape and the cross section of the thigh bone have irregular shapes. For simplicity, the cross section is assumed to be hollow circular and the shape of the two endings of the thigh bone is assumed to be identical at each end. **Table 3.3** shows the dimensions used to build the thigh bone model in addition to the mass and the center of gravity location. The model of the thigh bone is shown in **Figure 3.6**.

Table 3.3. Dimensions and specifications of the thigh bone model.

Parameters	**Values**
Length	0.464 m
Outer radius	0.045 m
Inner radius	0.035 m
Mass	5 kg
Center of gravity location as a percentage of the thigh length measured from the proximal ends	43.3 %

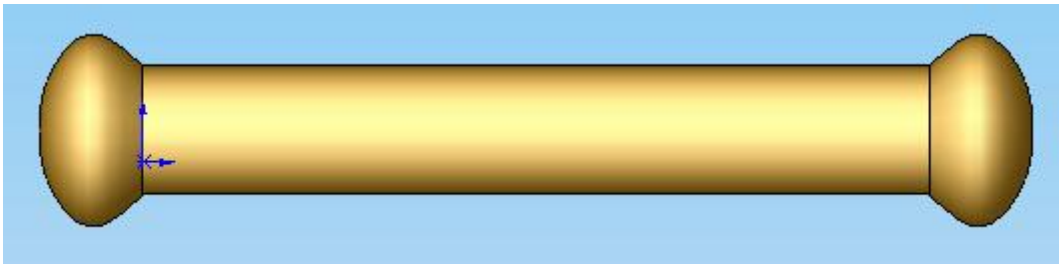

Figure 3.6. Thigh bone model.

The model shown in **Figure 3.6** is built using **SolidWorks 2004 SP04.2** [23] software. It can be noticed that the thigh bone is modeled as a rigid body. The model is imported to the **ADAMS** software, where it will be connected to the other bodies.

3.3 Foot Model

The geometrical shape of the foot bones is shown in **Figure 3.7** as depicted from the visible human viewer.

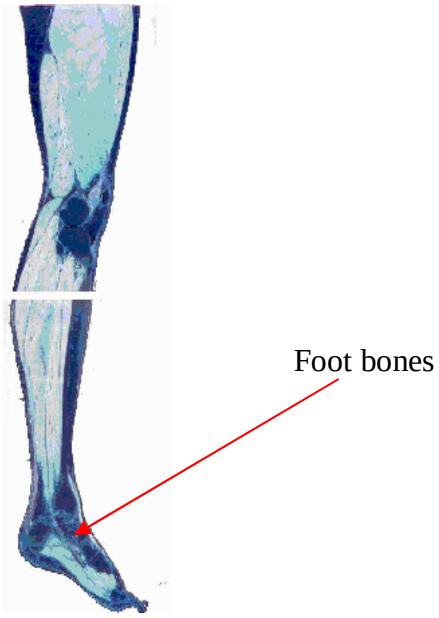

Figure 3.7. The geometrical shape of the foot bones [22].

It can be noticed from the previous figure that the foot bones have complex geometrical features. For simplicity, the foot bones are modeled as one rigid body. The foot model is built directly using **ADAMS** Software. **Table 3.4** shows the dimensions used to build the foot bone model in addition to the mass and the center of gravity location.

Table 3.4. Dimensions and specifications of the foot model.

Parameters	**Values**
Length	0.1 m
Height	0.05 m
Mass	1 kg
Center of gravity location as a percentage of the foot length measured from the proximal ends	50 %

3.4 Assembly of the Model

The complete model is assembled using **ADAMS** software. **Figure 3.9** shows the assembled lower limb model.

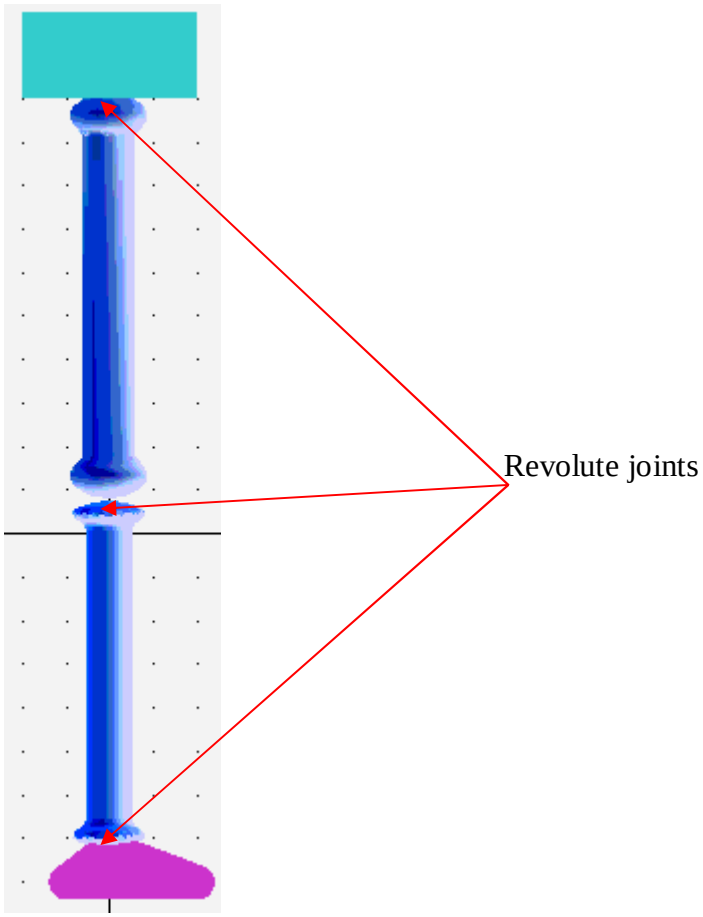

Figure 3.8. Lower limb model.

The three joints connecting the four bodies are modeled as revolute joints. The kinematic restrictions for each joint depend on the exercise to be applied to the model. The human body is modeled as rectangle with a mass equal to 30 kg. The mass of the upper body is based on the assumption that each leg will carry half of the upper human body weight. The muscles connected to the lower limb bones, can be modeled as forces between the bodies. However, only the active muscles concerned with the physical exercise can be taken into consideration. In the following chapter the model shown in **Figure 3.8** is investigated under raising the sole of the foot exercise, and only two muscles are being modeled.

4. NUMERICAL EXAMPLE

Raising the sole of the foot is considered one of the simplest and most common physical exercises the human can do. One cycle of the exercise is conducted by raising the sole of the foot. Consequently, the heel rises up from the ground until reaching a maximum height from it. Upon releasing the muscles of the lower limb, the heel hits the ground again and so on. In this chapter, the model of the lower limb built in the previous chapter is studied under this exercise. The most important muscles that control the movement in this exercise are gastrocnemius and soleus muscles. **Figure 4.1** show gastrocnemius and soleus muscles.

Gastrocnemius muscle Soleus muscle

Figure 4.1. Gastrocnemius and soleus muscles [24].

Some important specifications of the two muscles needed in the model are shown in **Table 4.1.**

Table 4.1. Specifications of the gastrocnemius and soleus muscles [24].

Specifications	**Gastrocnemius muscle**	**Soleus muscle**
Origin	Medial head from posterior nonarticular surface of medial femoral condyle; lateral head from lateral surface of femoral lateral condyle	Posterior aspect of fibular head, upper 1/4 - 1/3 of posterior surface of fibula, middle 1/3 of medial border of tibial shaft, and from posterior surface of a tendinous arch spanning the two sites of bone origin
Insertion	The two heads unite into a broad aponeurosis which eventually unites with the deep tendon of the soleus to form the achilles tendon, inserting on the middle 1/3 of the posterior calcaneal surface	Eventually unites with the gastrocnemius aponeurosis to form the achilles tendon, inserting on the middle 1/3 of the posterior calcaneal surface
Action	Powerful plantar flexor of ankle	Powerful plantar flexor of ankle

It can be noticed from the action of the two muscles mentioned in the previous table, that both of them are considered the main active muscles in moving the ankle joint. Gastrocnemius muscle is modelled as a force acting between the thigh and the foot, where the foot is the action body and the thigh is the reaction body. Soleus muscle is modelled as a force acting between the shank and the foot, where the foot is the action body and the thigh is the reaction body. Both forces have the same origin point on the foot and controlled via step function. **Figure 4.2** shows the step function control for the forces exerted from gastrocnemius and soleus muscles respectively for one cycle only.

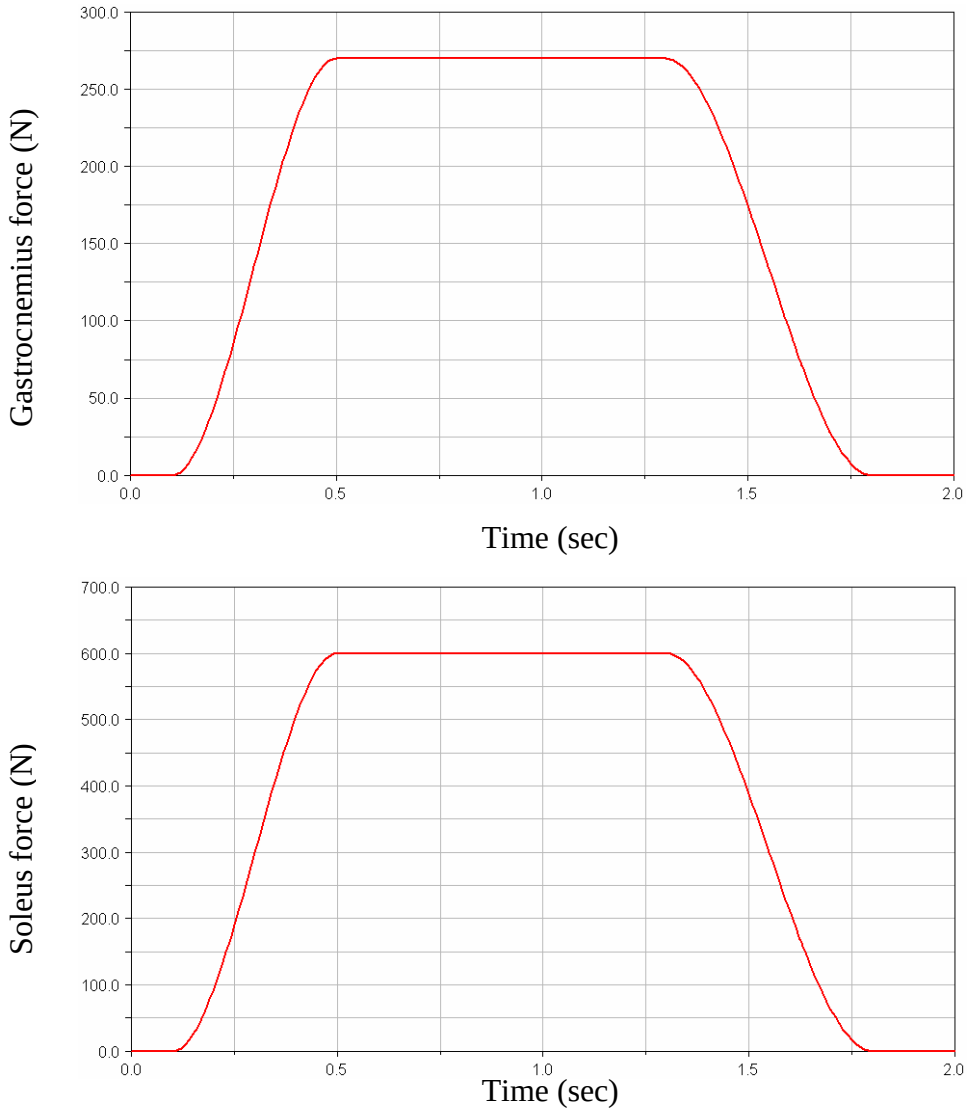

Figure 4.2. Step function control of the gastrocnemius and soleus forces for one cycle.

It can be noticed from the previous figure that the force exerted from the soleus muscle is larger than the force exerted from the gastrocnemius muscle. This is due to the fact that, the force production capacity from the muscle is determined by means of its physiological area. The ratio between the physiological area of the soleus muscle to the one of the gastrocnemius muscle equals to **230 : 96** [25]. One may notice also, the mechanism at which the exercise is conducted in which there are two pauses at each cycle of the exercise. First one occurs at the standing state, while the second one occurs when the heel reaches the highest point from the ground. The positions of the exercise in one cycle are shown in **Figure 4.3**.

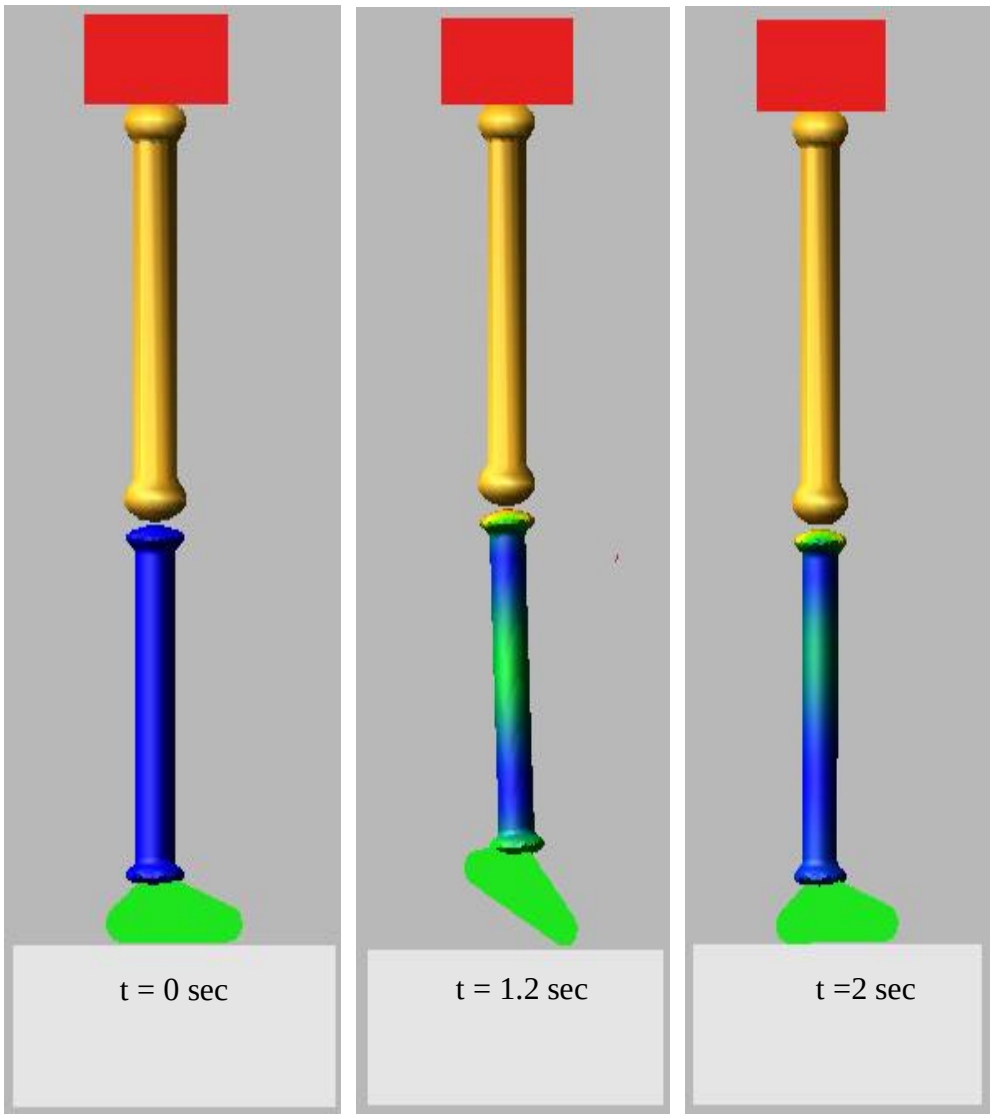

Figure 4.3. Positions of raising the sole of the foot exercise.

The modifications for the lower limb model when it experiences raising the sole of the foot exercise are shown in **Figure 4.4**.

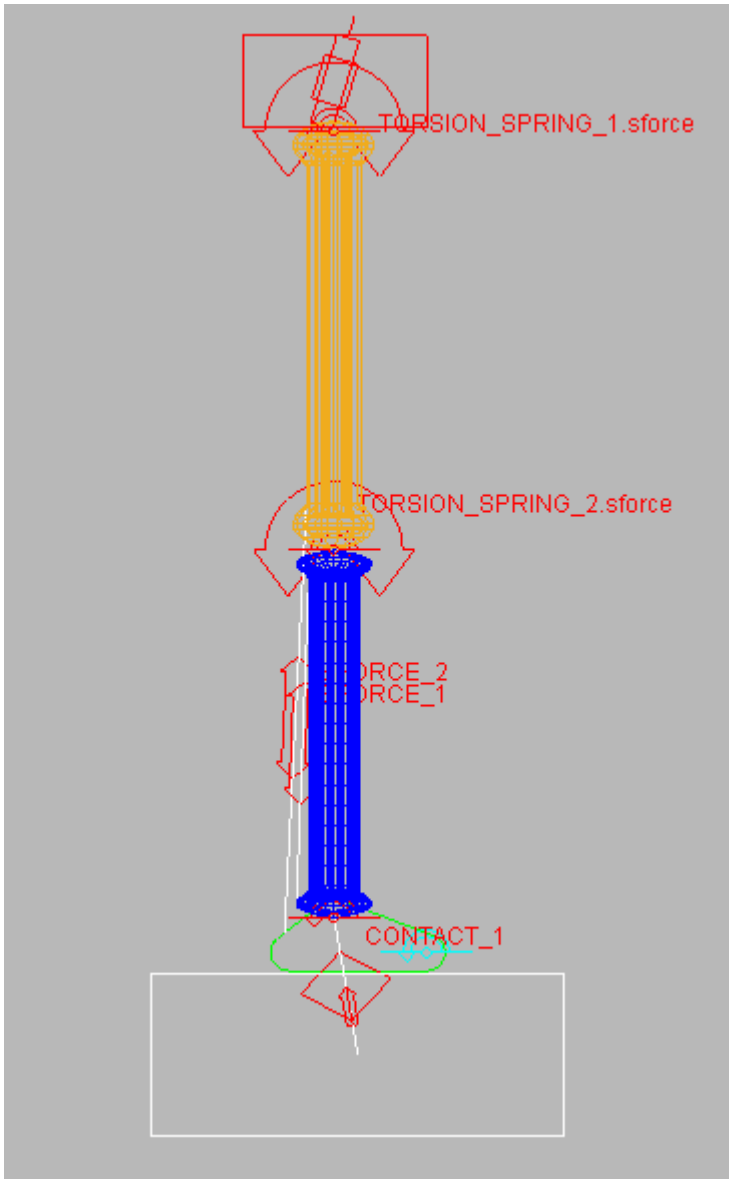

Figure 4.4. The lower limb model under raising the sole of the foot exercise.

It can be noticed from the previous figure that, two torsional spring forces have been added; one at the knee joint and the other one at the joint connecting the thigh with the body. This addition has been done to prevent the rotation for these two joints, as they are kept fixed during the exercise. SFORCE_1 represents the force exerted from the soleus muscle, while SFORCE_2 represents the force exerted from the gastrocnemius muscle. In reality, the human brain maintains the balance of the body through orders and instructions transferred to the muscles by a complicated central nervous system. In this model, the control system that includes the brain and central nervous system has not been modelled, thus a

transitional joint has been added between the body and the space, in the direction of the exercise movement. The function of this translational joint is to prevent the body from falling down while rising due to the gravitational force and maintains the body balance. To prevent the foot from sliding on the ground, a revolute joint has been added between the foot and the ground. Finally, the ground reaction force has been modelled as a contact force (CONTACT_1) between the foot and the ground. The specifications of this contact force is shown in **Table 4.2**.

Table 4.2. Specifications the contact force.

Specifications	**Values**
Type	Impact
Stiffness	1×10^{8} N/m
Damping	1×10^{5} Nsec/m
Force component	2.2
Penetration depth	1×10^{-4} m

4.1 Results and Discussion

The exercise simulation has been studied and tested at different simulation control parameters to check the behaviour of it. The simulation of the exercise has been carried out at the following step size values: 0.01, 0.001, 0.0001 and 0.00001. The model has shown logical behaviour at the different simulation control parameters, in which the variations between the results were negligible. However, the results shown in the following figures are measured for one exercise cycle, and at the following simulation control parameters; end time equals to 2 sec and step size equals to 0.01. Two nodes have been selected; one is located at the middle of the anterior shank bone and the other one is located at the middle of the posterior shank bone. The two nodes are located next to each other at the circular circumferential surface of the shank bone along the global X axis. **Figure 4.5** shows the locations of the selected nodes in the shank bone.

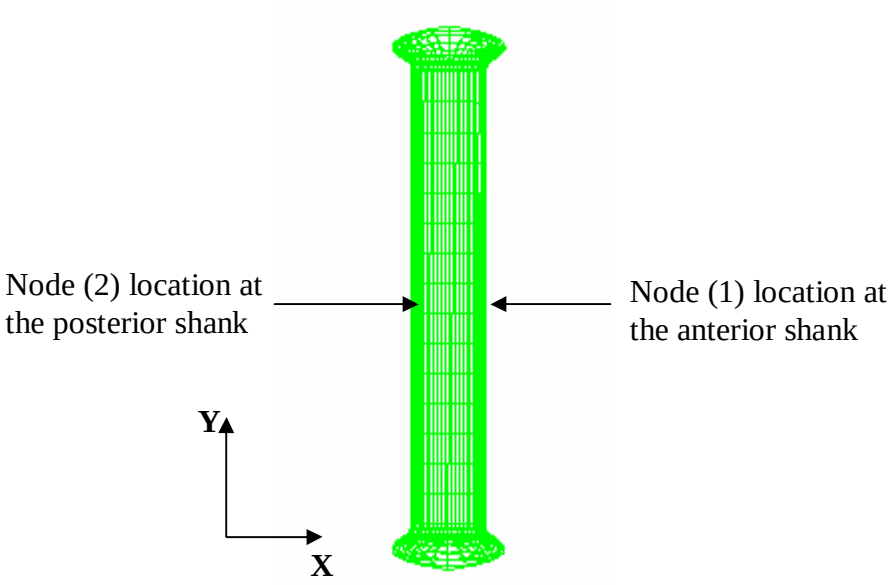

Figure 4.5. Nodes of interest in the shank bone.

In order to make a comprehensive analysis of the results shown in the previous figures, it is important to recognize the stresses concern in this physical exercise, which are; the pure compression and the bending moment stresses. The main stress is the bending moment, which is caused by the forces exerted from the soleus and gastrocnemius muscles. This stress takes place when the heel starts to rise from ground until it reaches to a maximum height from the ground. Due to this bending moment stress acting on the shank bone, the anterior shank will be in compression, while on the other hand, the posterior shank will be in tension. The pure compression stress is considered to have a minor deformation compared to the bending stress. This stress takes place during the standing still state at which the heel is on the ground. The ground reaction force, in addition to different strain and stress measurements at the two nodes shown in the previous figure with respect to the global coordinate system (**XY**) for one cycle of the exercise, are plotted in the following figures.

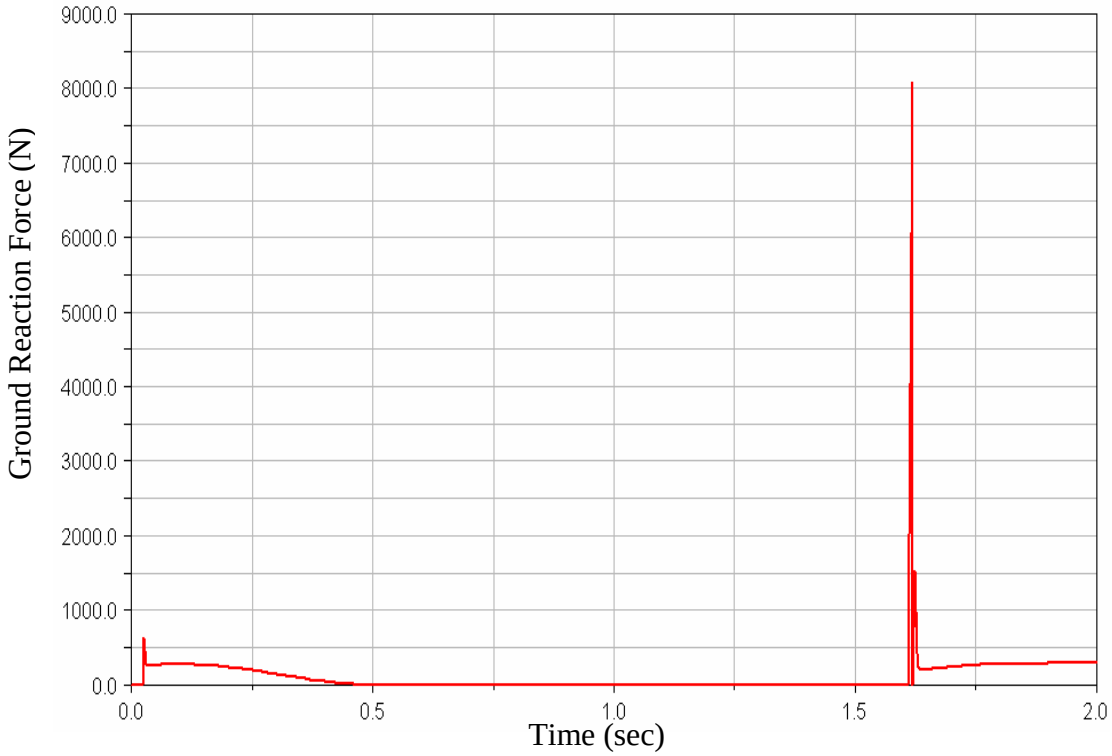

Figure 4.6. Ground reaction force magnitude.

In the previous figure, the magnitude of the ground reaction force is plotted. It can be noticed that the ground reaction force at the beginning of the exercise during the first standing still is equal to $\approx$650 N. While on the other hand, it increases steeply with a large amount as the heel hits the ground again. This is due to the momentum energy results from the movement of the body during the exercise. This leads to a high impact force as the heel hits the ground before the second standing still.

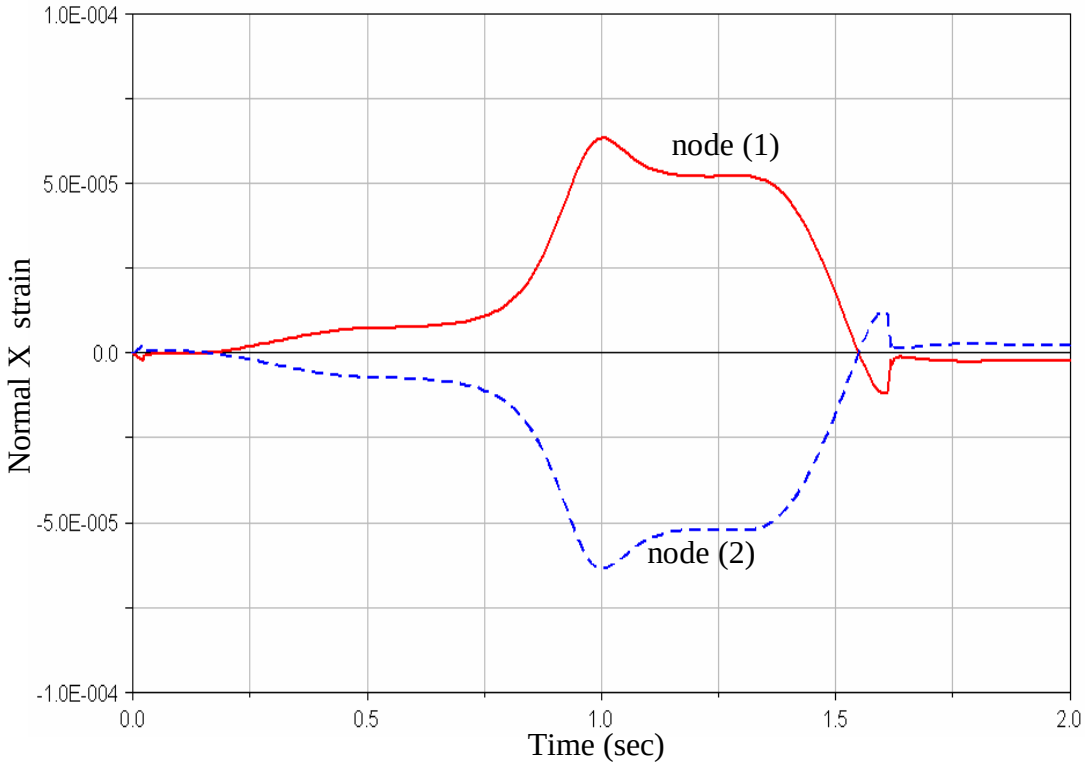

Figure 4.7. Normal X strain at the nodes (1) and (2).

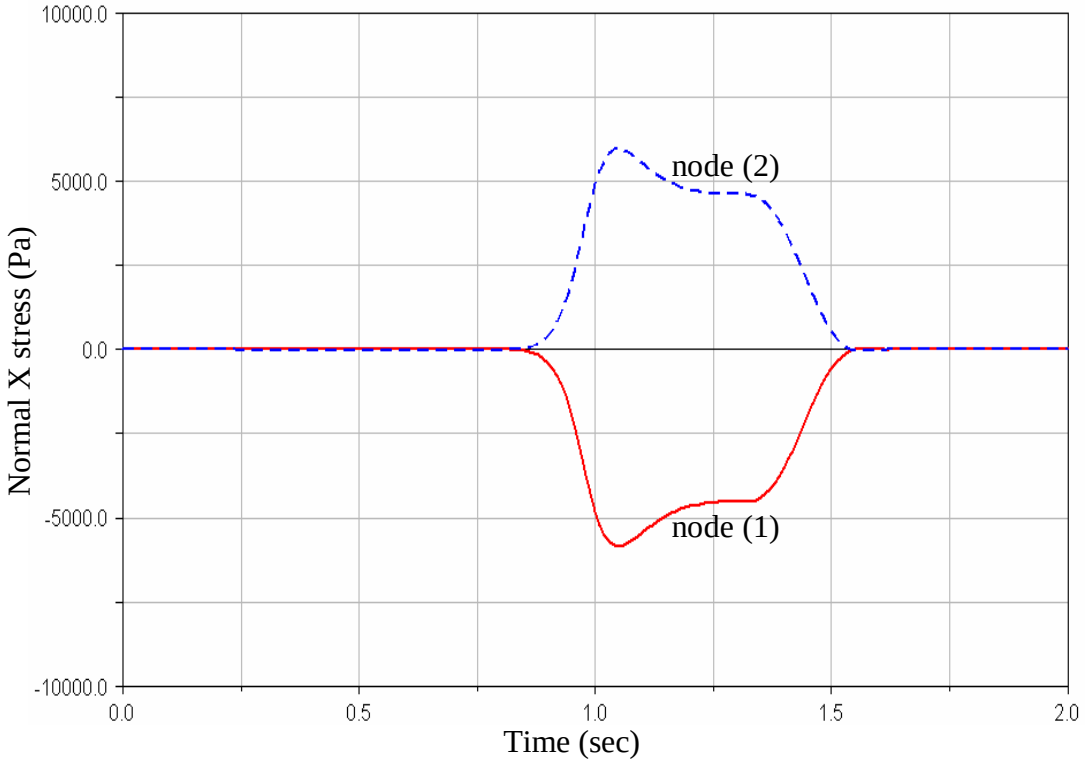

Figure 4.8. Normal X stress at the nodes (1) and (2).

In **Figure 4.7** and **Figure 4.8** the normal strains and stresses in X direction at the nodes (1) and (2) are plotted respectively. It can be noticed that the normal stress in X direction at the standing still state at the beginning and ending of the exercise at both nodes is equal to zero. This can be justified that, during the standing still state, the only stress acting is the pure compression which is in Y direction. While on the other hand, the normal strain in X direction at both nodes during the standing still state is not equal to zero. This can be explained that the pure compression stress in Y direction causes a strain in X direction. As a result of the bending moment stress, Node (1) experiences a compression stress, which causes a tensile normal strain in X direction. While on the other hand, node (2) experiences a tensile stress, which causes a compression normal strain in X direction.

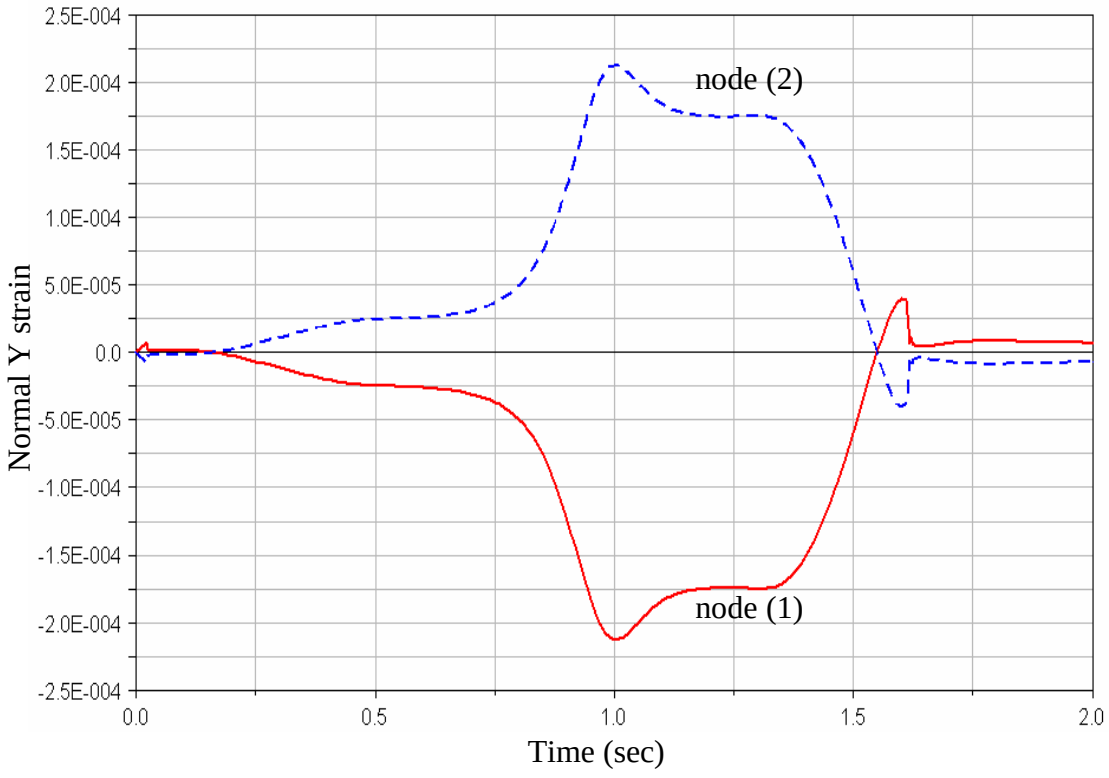

Figure 4.9. Normal Y strain at the nodes (1) and (2).

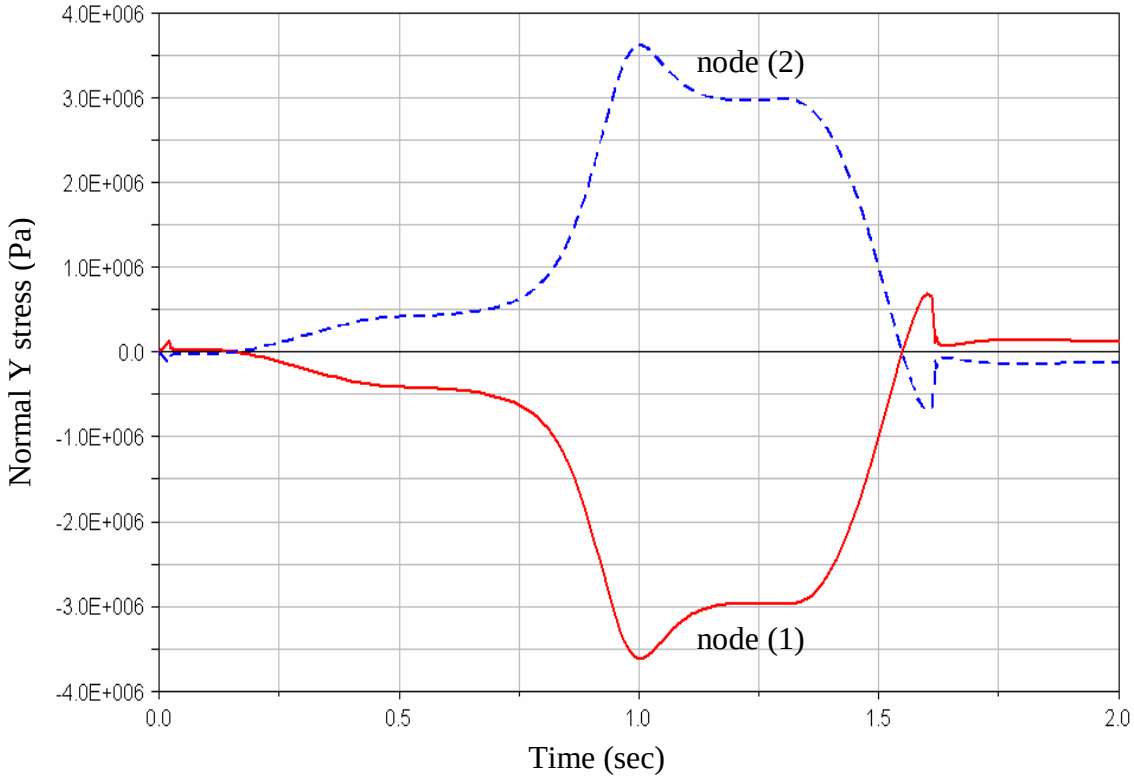

Figure 4.10. Normal Y stress at the nodes (1) and (2).

In **Figure 4.9** and **Figure 4.10** the normal strains and stresses in Y direction at the nodes (1) and (2) are plotted respectively. As a result of the bending moment stress, Node (1) experiences a compression stress, which causes a compression normal strain in Y direction. While on the other hand, node (2) experiences a tensile stress, which causes a tensile normal strain in Y direction. It can be noticed from **Figures (4.7, 4.9 and 4.10)** that the normal compression stress and thus the normal compression strain in Y direction, in addition to the normal strain in X direction at both nodes, experience a sudden change in direction as the heel hits the ground at the end of the exercise before the second standing still. This is due to the fact that the ground reaction force that causes the pure compression stress, increases incredibly as the heel hits the ground due to the momentum energy, which was shown previously in **Figure 4.6**.

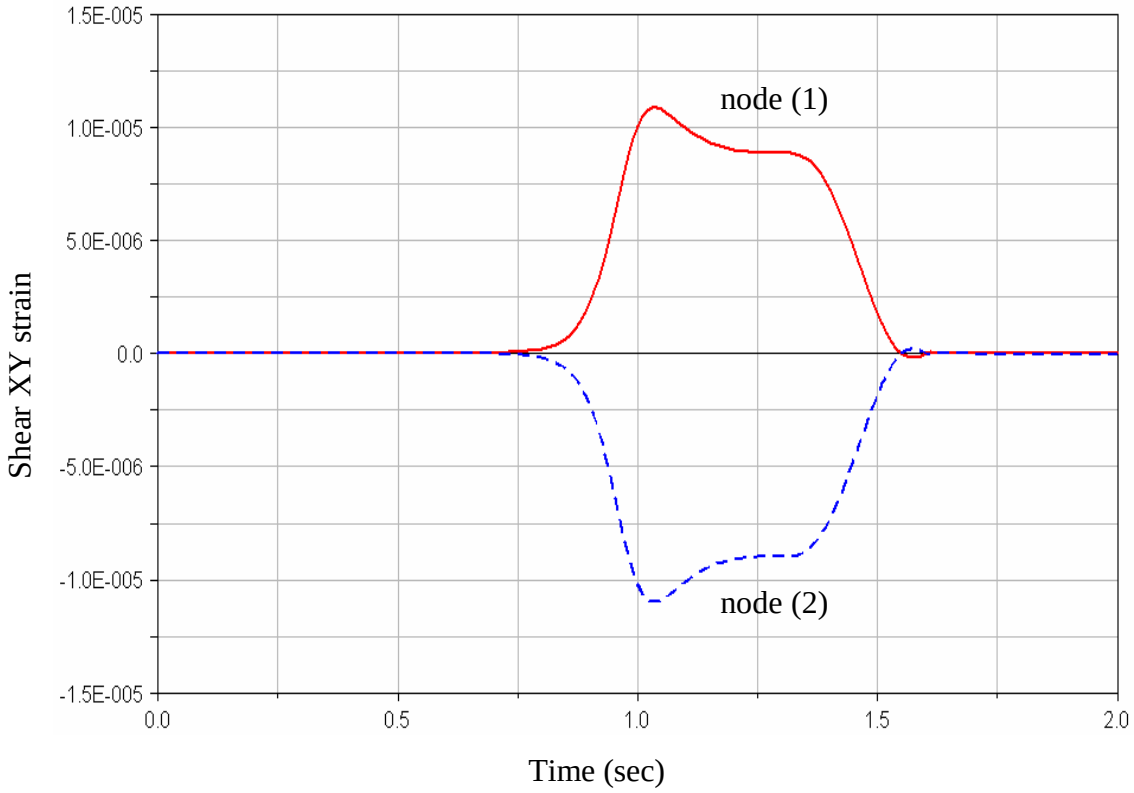

Figure 4.11. Shear XY strain at the nodes (1) and (2).

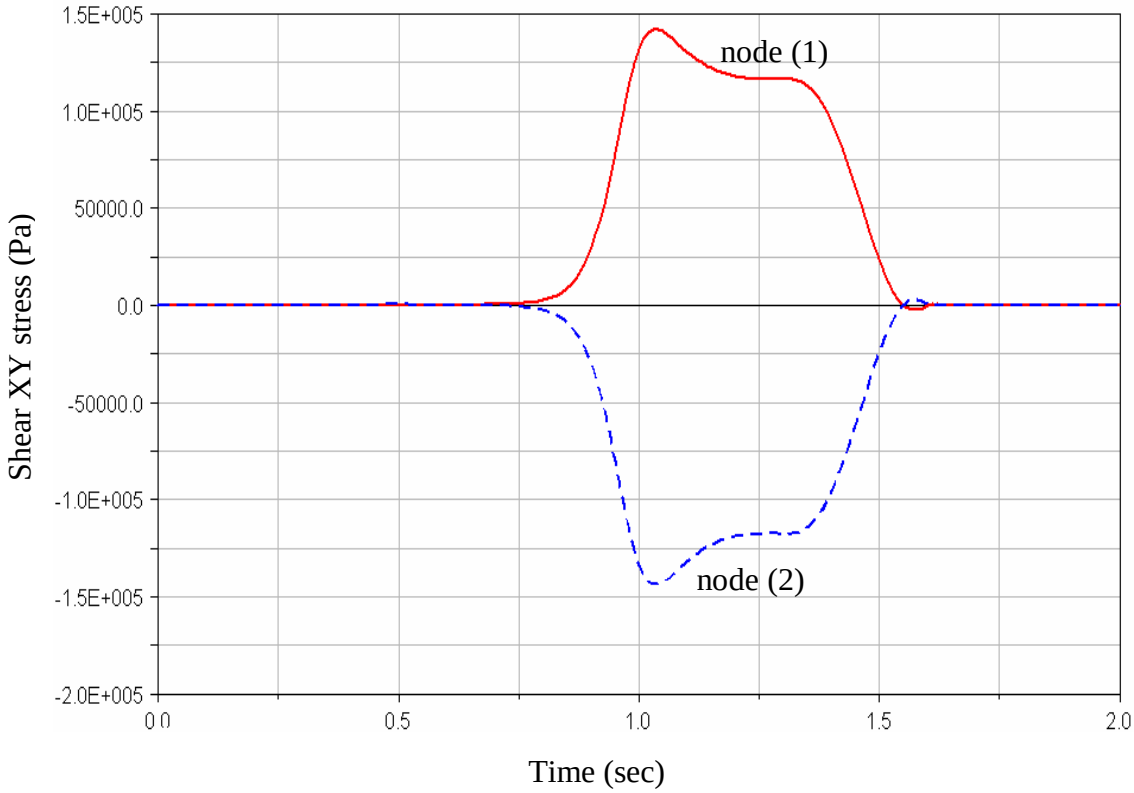

Figure 4.12. Shear XY stress at the nodes (1) and (2).

In **Figure 4.11** and **Figure 4.12** the shear strains and stresses in XY direction at the nodes (1) and (2) are plotted respectively. It can be noticed that the shear strain results from the bending moment stress only, as the compression XY shear stress is equal to zero. As a result of the bending moment, node (1) experiences a tensile XY shear strain, while node (2) experiences a compression XY shear strain. From **Figures (4.7-4.12)** some general comments can be noticed. First, as the heel reaches to maximum height from the ground, the stress and thus the strain curves plateau. This is due to the mechanism at which the exercise is conducted, in which there is a little pause as the heel reaches a maximum height from ground. Second, the strains result from the pure compression stresses are small compared to the strains result from the bending moment stress. This can be shown clearly in the following **Figures (4.13-4.16)** where the maximum and minimum principle strains and stresses at node (1) and (2) are plotted respectively.

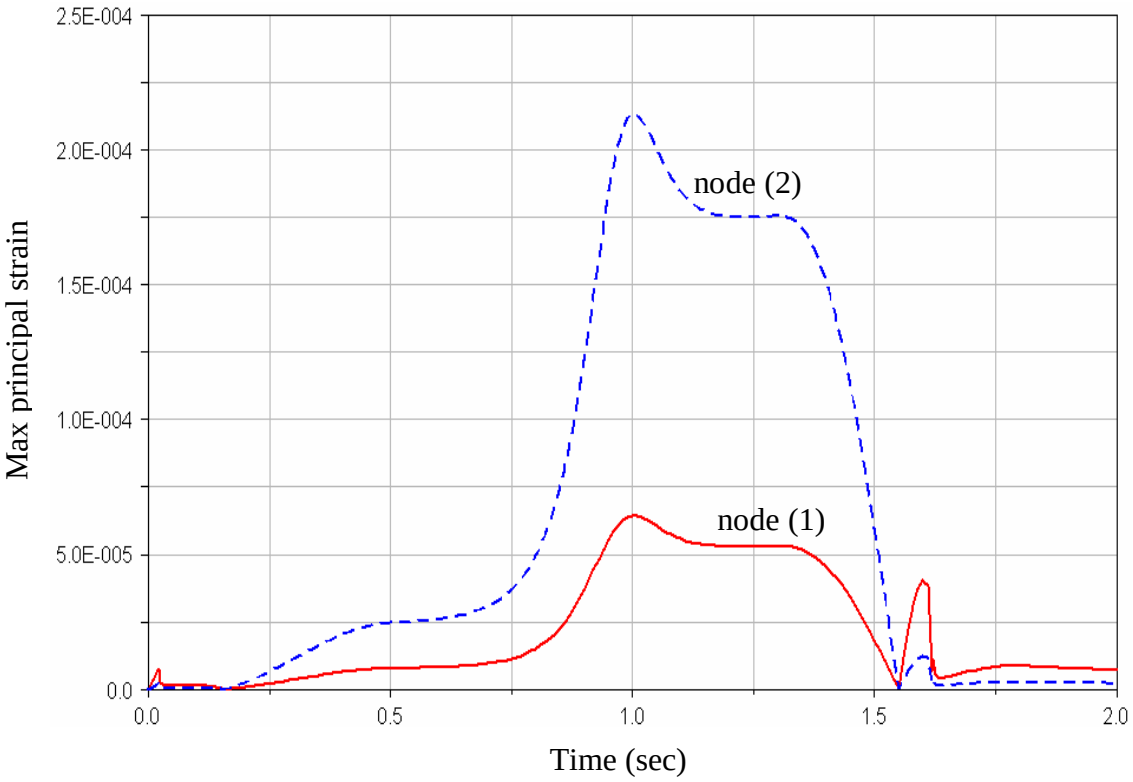

Figure 4.13. Maximum principal strain at the nodes (1) and (2).

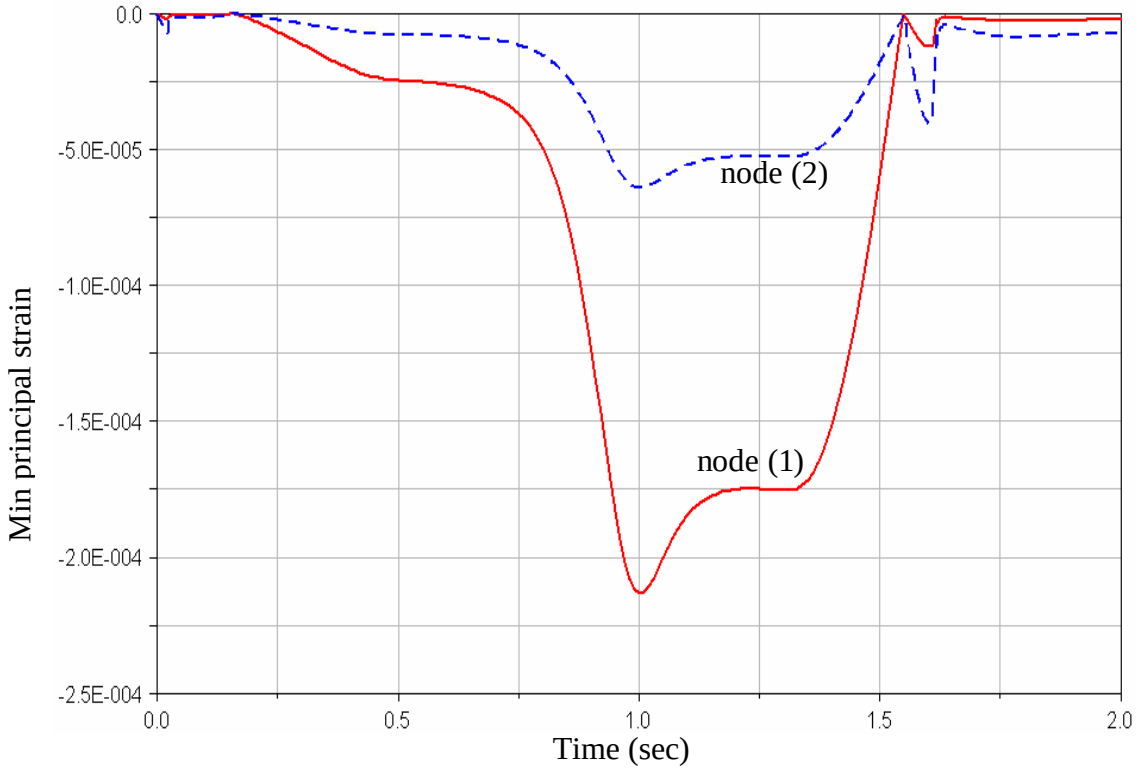

Figure 4.14. Minimum principal strain at the nodes (1) and (2).

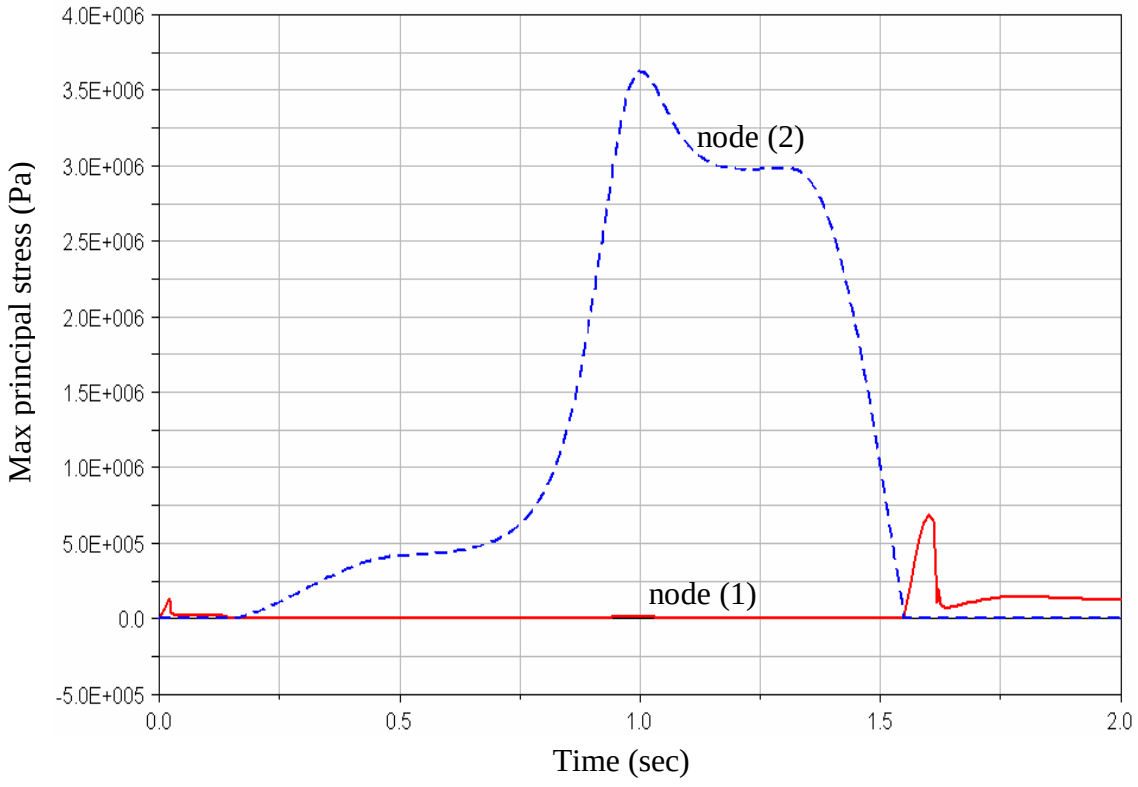

Figure 4.15. Maximum principal stress at the nodes (1) and (2).

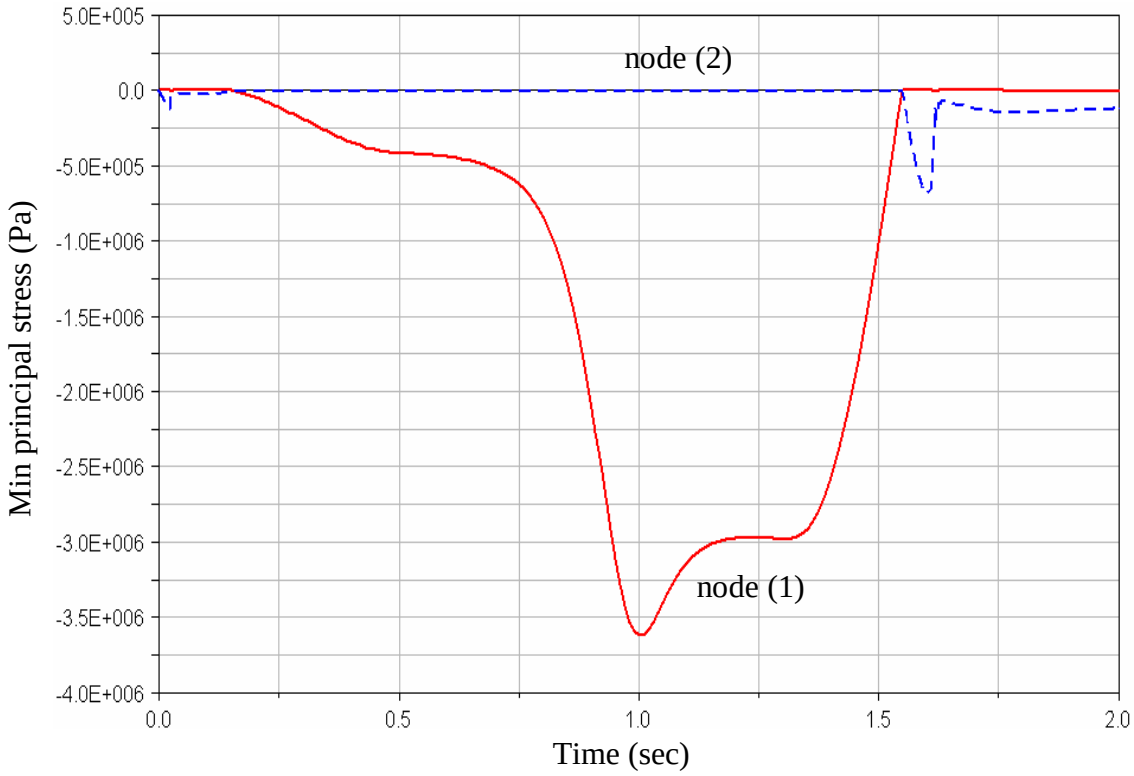

Figure 4.16. Minimum principal stress at the nodes (1) and (2).

From **Figure 4.13**, it can be noticed that the maximum principal strains at both nodes due to the bending moment stress are much higher than their magnitudes results from the pure compression stress. While on the other hand, from **Figure 4.14**, it can be noticed that the absolute magnitudes of the minimum principal strains at both nodes due to the bending moment stress are much higher than their absolute magnitudes results from pure compression stress. Third, the stress and thus strain results at nodes (1) and (2) are equal in magnitude and contrast in sign. The equality in magnitude is due to the fact that both nodes are located next to each others along the global X axis. While on the other hand, the contrast in sign results from the bending moment stress, thus node (1) will be in compression and node (2) in tension.

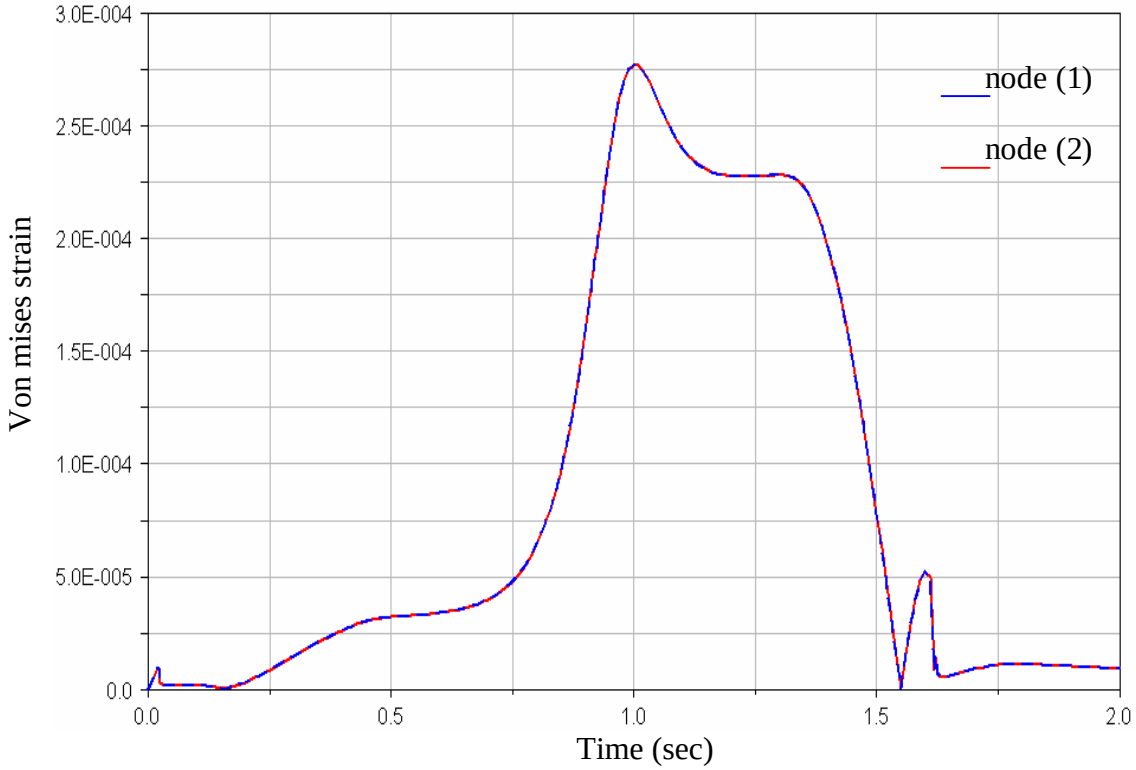

Figure 4.17. Von mises strain at the nodes (1) and (2).

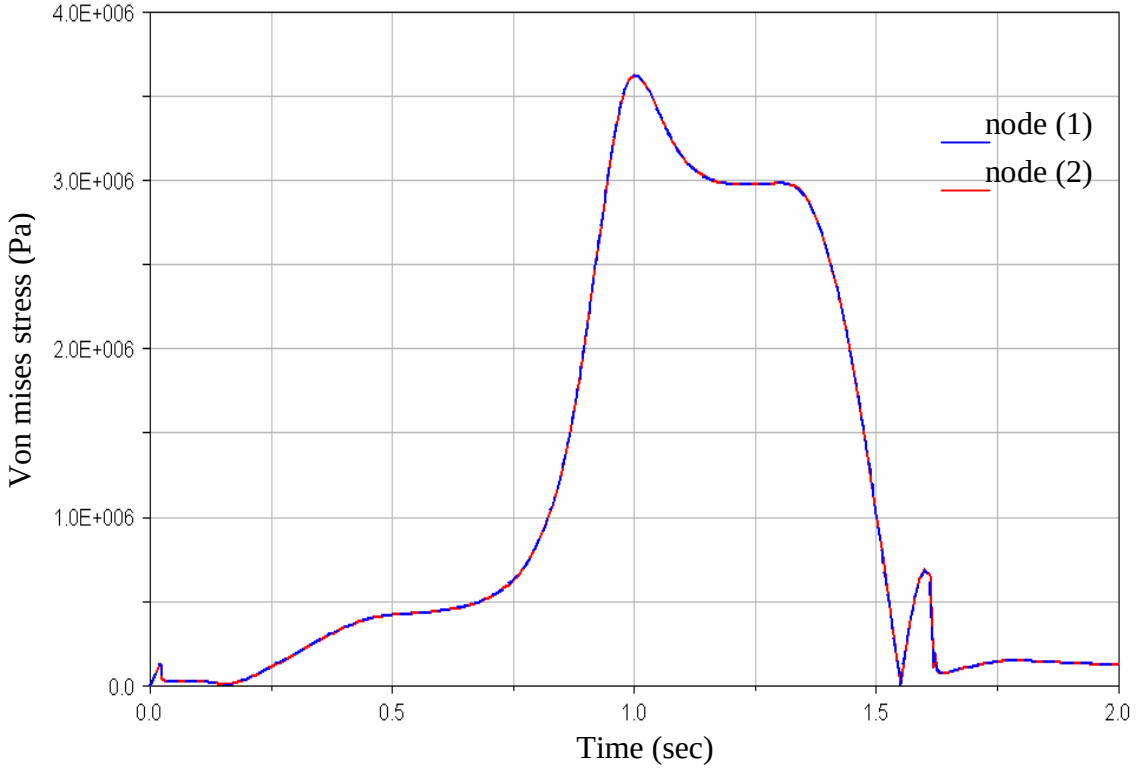

Figure 4.18. Von mises stress at the nodes (1) and (2).

In **Figure 4.17** and **Figure 4.18** von mises strains and stresses at the nodes (1) and (2) are plotted respectively. It can be noticed that they are equal at both nodes as the von mises stress is an expression of the stress in terms of normal and shear stresses. While on the other hand, the von mises strain is a strain expressed in terms of normal and shear strains.

The previous measurements of the maximum and minimum principle strains shown in **Figure 4.13** and **Figure 4.14** show good agreement with real strain measurements in **VIVO** (Latin expression refers to experimentation done on a living body). In Reference [26] the principle strains were measured in **VIVO** in an adult human shank during walking at level correspond to nodes (1) and (2). The maximum principle strain was equal to 437 *micro strain*, while the minimum principal strain was equal to -544 *micro strain*. In this model the maximum tensile strain, which corresponds to the maximum principle strain, occurs at node (2), and according to **Figure 4.13** it is equal to ≈ 212.5 *micro strain*. While on the other hand, the maximum compression strain, which corresponds to the minimum principal strain, occurs at node (1), and according to **Figure 4.14** it is equal to ≈-212.5 *micro strain*. In this model, the maximum principal strain equals to the minimum principal strain, as both nodes are located exactly next to each other along the global **X** axis. However, walking is considered more strenuous than rising the sole of the foot exercise. This leads to a result, that the multibody dynamic approach is considered a powerful tool in modelling human skeletal.

5. CONCLUSION

The aim of this study is to prove the efficiency and capability of the flexible multibody dynamic approach in measuring the strain in the human lower limb bones resulted from different exercises. The bone strain plays major role in the battle against the metabolic bone diseases, as the absolute strain increment is considered one of the important factors in increasing the bone strength. The main motivation in using multibody dynamic approach in modelling the human lower limb is the difficulty of obtaining different important measurements such as muscle forces and bone strain directly from the human by means of invasive techniques. To satisfy the aim of this study, the human lower limb is modelled using multibody dynamic approach. The model consists of three bodies; the thigh, the shank and the foot. The shank is considered to be flexible while the other bodies are considered to be rigid. Floating frame of reference formulation was used to account for the flexibility in the shank. The model was tested and verified through a numerical example showing raising the sole of the foot exercise. In this study, a commercial multibody simulation code (**ADAMS**) was used to accomplish the model. The strain was measured in the middle of the shank, and the results have shown good agreement with the real strain measurements in **VIVO** (Latin expression refers to experimentation done on a living body) in the shank taken at the same location. According to this study presented in this thesis, the multibody dynamic approach can be seen as a promising and challenging tool in modelling human skeletal from three points of views. First, modelling and simulation can provide information that is not directly accessible by experimentation on humans. Second, the model simulation data can be very helpful in explaining the results obtained from the motion analysis experiment. Third, the flexible multibody model of the human lower limb can be used to design several physical training exercises to achieve the optimal strength of the bones. For example, the model presented in chapter three can be improved and extended to be used in developing different exercises in order to maintain or increase the bone strength.

The results obtained from the previous example, show that the theory and method used in introducing the flexibility is potentially utilizable in human bone modelling. In addition, they demonstrate a good functionality and suitability of the floating frame of reference formulation for the computationally efficient and realistic modelling of the human bones. In the future, a more detailed and complex model of the human lower limb bones can be built in three dimensions. In this model a detailed description of the muscles, joints and tendons can be done. Moreover, further studies can be conducted in modelling the control system that includes the brain and central nervous system. The control system is very important in controlling the muscles and thus obtaining the desirable movement of the lower limb model. This detailed lower limb model can be utilized in designing several physical exercises to achieve the optimal bone strength.

REFERENCES

[1] C. Kraus, H. G. Bock, H. Mutschler, Parameter Estimation For Biomechanical Models Based on a Special Form of Natural Coordinates *Multibody System Dynamics* **13** (2005) 101-111

[2] M. P. T. Silva, J. A. C. Ambrósio, Kinematic Data Consistency in the Inverse Dynamic Analysis of Biomechanical Systems, *Multibody System Dynamics* **8** (2002) 219-239.

[3] T. Spägele, A. Kistner, A. Gollhofer, Modelling Simulation and Optimization of a Human Vertical Jump, *Journal of Biomechanics* **32** (1999) 521-530.

[4] W. M. Kohrt, S. A. Bloomfield, K. D. Little, M. E. Nelson, V. R. Yingling, American College of Sports Medicine Position Stand: Physical Activity and Bone Health, *Med SciSports Exerc* **36** (2004) 1985-1996.

[5] Y. Bei, B. Fregly, Multibody Dynamic Simulation of Knee Contact Mechanics, *Medical Engineering & Physics* **26** (2004) 777-789.

[6] M. P. T. Silva, J. A. C. Ambrosio, M. S. Pereira, Biomechanical Model With Joint Resistance For Impact Simulation, *Multibody System Dynamics* **1** (1997) 65-84.

[7] T. Pressel, M. Lengsfeld, Functions of Hip Joint Muscles, *Medical engineering & Physics* **20** (1998) 50-56.

[8] E. Pennestri, A. Renzi, P. Santonocito, Dynamic Modelling of Human Arm With Video- Based Experimental Analysis, *Multibody System Dynamics* **7** (2002) 389-406.

[9] W. Blajer, Contact Modelling and Identification of Planar Somersaults on the Trampoline, *Multibody System Dynamics*, **10** (2003) 289-312.

[10] Y. Nakamura, K. Yamane, Y. Fujita, I. Suzuki, Somatosensory Computation For Man-Machine Interface From Motion-Capture Data and Musculoskeletal Human Model, *IEE Transactions on Robotics*, **21** (2005) 58-66.

[11] M. P. T. Silva, J. A. C. Ambrósio, Kinematic Data Consistency in the Inverse Dynamic Analysis of Biomechanical Systems," *Multibody System Dynamics* **8** (2002) 219-239.

[12] T. Gordon, R. Hopkins, Parametric Identification of Multibody Models For Crash Victim Simulation, *Multibody System Dynamics*, **1** (1997) 58-112.

[13] B. Fox, L. S, Jennings, A. Y. Zomaya, Numerical Computation of Differential-Algebraic Equations For Nonlinear Dynamics of Multibody Android System in Automobile Crash Simulation, *IEEE Transaction of Biomechanical Engineering*, **46** (1999) 1199-1206.

[14] A.A. Shabana, Dynamics of Mutlbody Systems, 2 nd ed, Cambridge University Press, 1998.

[15] A.A. Shabana, Vibration of Discrete and Continuous Systems, 2 nd ed, Springer, Inc. 1996.

[16] T. M. Wasfy, A. K. Noor, 2003, Computational Strategies For Flexible Multibody Dynamics, *Applied Mechanics Reviews* **1** (2003) 553-613.

[17] H. El-Absy, A. A. Shabana, Coupling Between Rigid Body and Deformation Modes, *Journal of Sound and Vibration* **198** (5) (1996) 617-637.

[18] A. A. Shabana, Resonance Conditions and Deformable Body Co-ordinate Systems, *Journal of Sound and Vibration* **192** (1) (1996) 389-398.

[19] ANSYS User's Manual, 2001, Theory, Twelfth Edition, SAS IP, Inc. ©.

[20] R. R. Craig and M. C. C. Bampton. Coupling of Substructures For Dynamic Analysis, *American Institute of Aeronautics and Astronautics Journal*, **6** (7) (1968) 1313-1319.

[21] ADAMS Online Documentation, 2001, version 12.0, Mechanical Dynamics, Inc, Ann Arbor, Michican, USA.

[22] National Library of Medicine, The Visible Human Project [e-document]. January 1st 1996, [retrieved August 10th 2006]. From: http://www.nlm.nih.gov/research/visible/visible_human.html

[23] SolidWorks Online User's Guide, 2005, Theory, Educational Edition.

[24] L. Michael, M. D. Richardson, Lower Extremity Muscle Atlas [e-document].
1997, [retrieved August 5th 2006]. From:
http://www.rad.washington.edu/atlas2/

[25] A. T. Fukunaga, Physiological Cross-Sectional Area of Human Leg Muscles Based on Magnetic Resonance Imaging, *Journal of Orthopaedic Research* **10** (6) (1992) 34-928.

[26] D. B. Burr, I C. Milgrom, D. Fyhrie, M. Forwood, M. Nyska, A. Finestone, S. Hoshaw, E. Salag, A. Simkin, In Vivo Measurement of Human Tibial Strains During Vigorous Activity, *Bone* **18** (5) (1996) 405-410.